A homeostatic interferon-lambda response to bacterial microbiota stimulates preemptive antiviral defense within discrete pockets of intestinal epithelium

Authors: Jacob A. Van Winkle[1], Stefan T. Peterson[2], Elizabeth A. Kennedy[2], Michael J. Wheadon[2], Harshad Ingle[2], Chandni Desai[3], Rachel Rodgers[2,4], David A. Constant[1], Austin P. Wright[1], Lena Li[1], Maxim Artyomov[3], Sanghyun Lee[2], Megan T. Baldridge[2,5#], and Timothy J. Nice[1#]

Affiliations:

[1] Department of Molecular Microbiology and Immunology, Oregon Health and Science University, Portland, OR 97239, USA

[2] Division of Infectious Diseases, Department of Medicine, Edison Family Center for Genome Sciences & Systems Biology, Washington University School of Medicine, St. Louis, MO 63110, USA

[3] Division of Immunobiology, Department of Pathology and Immunology, Washington University School of Medicine, St. Louis, MO 63110, USA

[4] Department of Pediatrics, Washington University School of Medicine, St. Louis, MO 63110, USA

[5] Department of Molecular Microbiology, Washington University School of Medicine, St. Louis, MO 63110, USA

[#]Correspondence to: nice@ohsu.edu (T.J.N.), mbaldridge@wustl.edu (M.T.B.)

Abstract

Interferon-lambda (IFN-λ) protects intestinal epithelial cells (IECs) from enteric viruses by inducing expression of antiviral IFN-stimulated genes (ISGs). Here, we find that bacterial microbiota stimulate a homeostatic ISG signature in the intestine of specific pathogen-free mice. This homeostatic ISG expression is restricted to IECs, depends on IEC-intrinsic expression of IFN-λ receptor (*Ifnlr1*), and is associated with IFN-λ production by leukocytes. Strikingly, imaging of these homeostatic ISGs reveals localization to pockets of the epithelium and concentration in mature IECs. Correspondingly, a minority of mature IECs express these ISGs in public single-cell RNA sequencing datasets from mice and humans. Furthermore, we assessed the ability of orally-administered bacterial components to restore localized ISGs in mice lacking bacterial microbiota. Lastly, we find that IECs lacking *Ifnlr1* are hyper-susceptible to initiation of murine rotavirus infection. These observations indicate that bacterial microbiota stimulate ISGs in localized regions of the intestinal epithelium at homeostasis, thereby preemptively activating antiviral defenses in vulnerable IECs to improve host defense against enteric viruses.

Introduction

Interferons (IFNs) are a family of cytokines produced in response to infection that signal IFN receptor-bearing cells to induce transcription of hundreds of interferon-stimulated genes (ISGs). These ISGs perform diverse functions, but many cooperate to induce an antiviral state (Sadler and Williams, 2008; Schoggins and Rice, 2011). There are three types of IFNs: type I IFNs (IFN-αs, IFN-β, others), type II IFN (IFN-γ), and type III IFNs (IFN-λs). These three types are differentiated by receptor usage (type I IFN receptor: *Ifnar1*/*Ifnar2*; type II IFN receptor: *Ifngr1*/*Ifngr2*; type III IFN receptor: *Ifnlr1*/*Il10rb*), but all three receptor complexes signal through Janus-kinase (JAK) and signal transducer and activator of transcription (STAT) factors to stimulate ISG transcription (Ingle et al., 2018; Schneider et al., 2014). Type I and III IFNs are directly stimulated by host detection of microbe-associated molecular patterns (MAMPs) such as viral nucleic acids, and the prominent contribution of these IFN types to antiviral defense is reflected by the breadth of evasion strategies used by diverse viral families to prevent their production or action (Levy and García-Sastre, 2001; Rojas et al., 2021; Taylor and Mossman, 2013). The type I IFN receptor is expressed broadly across most cell types, whereas the type III IFN receptor, *Ifnlr1,* is primarily restricted to epithelial cells (Kotenko and Durbin, 2017; Sommereyns et al., 2008). Accordingly, IFN-λ is of particular importance in effective antiviral defense of barrier tissues.

Interestingly, previous studies in mice have noted that intestinal epithelial cells (IECs) are hyporesponsive to type I IFN (Lin et al., 2016; Mahlakõiv et al., 2015; Pott et al., 2011; Van Winkle et al., 2020). The responsiveness of IECs to type I IFN appears to be developmentally regulated because the IECs of adult mice exhibit weaker type I responses than IECs of neonatal mice (Lin et al., 2016). Additionally, infection of mice deficient in IFN receptors (*Ifnar1*, *Ifngr1*, *Ifnlr1*; single or double knockouts) with enteric viruses indicates that IFN-λ is the predominant antiviral IFN type that controls viral replication in the gastrointestinal epithelium (Mahlakõiv et al., 2015; Nice et al., 2015; Pott et al., 2011). IECs can robustly respond to IFN-λ with upregulation of canonical antiviral

60 ISGs and increased resistance to infection by enteric viruses, such as rotaviruses and noroviruses
61 (Baldridge et al., 2017; Nice et al., 2015; Pott et al., 2011). Mouse rotavirus (mRV) is a natural
62 pathogen of mice that infects enterocytes located at the tips of villi in the small intestine (Burns et
63 al., 1995). Rotaviruses have developed mechanisms to antagonize the induction of IFN by
64 infected cells, suggesting that evasion of the IFN response is necessary for efficient epithelial
65 infection (Arnold et al., 2013). Indeed, prophylactic administration of IFN-λ significantly reduces
66 the burden of mRV infection, demonstrating its potential for mediating epithelial antiviral immunity
67 to this pathogen (Hernández et al., 2015; Lin et al., 2016; Pott et al., 2011; Van Winkle et al.,
68 2020). However, a protective role of the endogenous IFN-λ response to mRV infection is less
69 clear, perhaps reflecting the success of mRV evasion mechanisms.

70 Epithelial immunity in the gut must be appropriately balanced to protect the intestinal
71 epithelium while preventing loss of barrier integrity and intrusion by microbes that are abundant
72 within the gastrointestinal tract. The bacterial microbiota in the intestine perform critical functions
73 by aiding in host metabolism (Krajmalnik-Brown et al., 2012), providing a competitive environment
74 to defend against pathogens (Kim et al., 2017), and initiating and maintaining host immune
75 function during homeostasis (Honda and Littman, 2016; Rooks and Garrett, 2016). In this complex
76 environment host epithelial and immune cells detect bacteria and viruses using a suite of pattern
77 recognition receptors (PRRs) that sense the presence of MAMPs. Stimulation of PRRs, such as
78 the toll-like receptor (TLR) family, activates antimicrobial and antiviral defenses providing local
79 protection in many tissues (Chu and Mazmanian, 2013; Iwasaki and Medzhitov, 2015; Thompson
80 et al., 2011). TLR-dependent pathways induce production of IFNs, primarily by signaling through
81 TIR-domain-containing adapter-inducing interferon-β (TRIF) and myeloid differentiation primary
82 response 88 (MYD88) adapter proteins (Monroe et al., 2010; Odendall et al., 2017), providing a
83 mechanism by which bacterial MAMPs can initiate IFN responses.

84 Signals from the bacterial microbiota have been shown to elicit a steady-state type I IFN
85 response in systemic tissues and cell types that can prime antiviral immunity by several

independent studies (Abt et al., 2012; Bradley et al., 2019; Ganal et al., 2012; Steed et al., 2017; Stefan et al., 2020; Winkler et al., 2020). Additionally, a steady-state ISG signal has been observed in the intestine of uninfected mice (Baldridge et al., 2015; Lin et al., 2016; Stockinger et al., 2014), but this intestinal response remained poorly characterized. Together with the observed hypo-responsiveness of IECs to type I IFN, these findings suggested that bacterial microbiota may stimulate an IFN-λ response in the gut. To explore this interaction, we undertook the present study to assess the role of bacterial microbiota in induction of enteric ISGs at homeostasis using a combination of broad-spectrum antibiotics (ABX) and genetically modified mice.

In this study, we uncovered an ISG signature in IECs that was dependent on the presence of bacteria and IFN-λ signaling (hereafter referred to as 'homeostatic ISGs'). This panel of genes was present in WT mice with conventional microbiota and was reduced in WT mice treated with ABX and in mice lacking *Ifnlr1*. We revealed that homeostatic ISG expression is i) restricted to the intestinal epithelium across both the ileum and colon, ii) independent of type I IFN signaling, and iii) associated with IFN-λ transcript expression by epithelium-associated CD45+ leukocytes. Surprisingly, we found that homeostatic ISGs are not expressed uniformly by all IECs; rather, expression is concentrated in localized pockets of IECs and in differentiated IECs relative to crypt-resident progenitors. These patterns of localized ISG expression are corroborated by independently-generated single-cell RNA sequencing data from mouse and human IECs. We also found that ISG expression can be increased in ABX-treated mice by reconstitution of bacterial microbiota or administration of bacterial lipopolysaccharide (LPS). Finally, we found that this microbiota-stimulated ISG signature provides protection from initiation of mRV infection. Cumulatively, this study found that bacteria initiate preemptive IFN-λ signaling in localized areas to protect IECs from enteric viruses.

Results

Bacterial microbiota stimulate IFN-λ response genes in the ileum at homeostasis

To determine the effect of bacterial microbiota on homeostatic IFN-λ responses, we compared gene expression in whole ileum tissue for the following experimental groups: i) wild-type C57BL/6J (WT) mice intraperitoneally-injected with IFN-λ as compared to unstimulated WT mice, ii) WT mice with conventional microbiota as compared to WT mice treated with an antibiotic cocktail (ABX) to deplete bacteria, iii) WT mice with conventional microbiota as compared to *Ifnlr1*$^{-/-}$ mice with conventional microbiota, and iv) *Ifnlr1*$^{-/-}$ mice with conventional microbiota compared to *Ifnlr1*$^{-/-}$ mice treated with ABX (**Figure 1A**). To rule out contributions of *Ifnlr1* toward an altered intestinal bacterial microbiota, we performed 16S rRNA sequencing on stool from *Ifnlr1*$^{+/+}$, *Ifnlr1*$^{+/-}$, and *Ifnlr1*$^{-/-}$ mice and did not find statistically significant differences in alpha-diversity and beta-diversity measurements with the statistical power available from 12 mice per group (**Figure S1**). For each comparison of ileum gene expression shown in **Figure 1A,** we performed gene-set-enrichment-analysis (GSEA) to determine enrichment or depletion of hallmark gene sets (Liberzon et al., 2016). The hallmark gene set that was most enriched in IFN-λ-treated WT mice compared to unstimulated WT mice was INTERFERON_ALPHA_RESPONSE (**Figures S2, 1B**). Therefore, this gene set reflects differences in IFN-λ responses between experimental conditions.

To deplete bacterial microbiota, we administered a cocktail of broad-spectrum antibiotics, and demonstrated that this treatment reduced bacterial 16S gene copies in stool to below the limit of detection (**Figure S3)**. GSEA of WT mice treated with ABX showed a significant depletion (negative enrichment score) of INTERFERON_ALPHA_RESPONSE hallmark genes in the ileum relative to WT mice with conventional microbiota (**Figure 1C**). These data indicate that ISGs are present at steady-state in the ileum of specific-pathogen-free mice with conventional microbiota and suggest that microbiota stimulate expression of these genes in the ileum at homeostasis.

Type I, II, and III IFN responses have substantial gene expression overlap; therefore, to prove that the IFN-λ receptor was necessary for expression of ISGs at homeostasis, we analyzed

135 gene expression in the ileum of *Ifnlr1*$^{-/-}$ mice. Indeed, GSEA showed significant reduction of
136 INTERFERON_ALPHA_RESPONSE hallmark genes in the ileum of *Ifnlr1*$^{-/-}$ mice compared to WT
137 mice (**Figure 1D**). Furthermore, expression of INTERFERON_ALPHA_RESPONSE hallmark
138 genes was not significantly decreased in *Ifnlr1*$^{-/-}$ mice treated with ABX compared to *Ifnlr1*$^{-/-}$ mice
139 with conventional microbiota (**Figure 1E**). In contrast to INTERFERON_ALPHA_RESPONSE,
140 other hallmark gene sets such as INFLAMMATORY_RESPONSE and
141 IL6_JAK_STAT3_SIGNALING were significantly decreased by ABX treatment in both WT mice
142 and *Ifnlr1*$^{-/-}$ mice (**Figure S2**), which indicates a selective requirement for *Ifnlr1* to elicit ISGs and
143 a minimal effect of *Ifnlr1*-deficiency on other microbiota-dependent genes. Together, these
144 findings suggest that *Ifnlr1* is necessary for the bacterial microbiota-dependent expression of ISGs
145 in the ileum at homeostasis. Since ISGs are enriched in mice upon IFN-λ stimulation and are
146 decreased in *Ifnlr1*$^{-/-}$ and ABX-treated mice, we conclude that the bacterial microbiota stimulates
147 IFN-λ responses in the ileum at homeostasis.

148 To define a core set of bacterial microbiota-dependent, *Ifnlr1*-dependent 'homeostatic
149 ISGs', we determined the overlap of differentially expressed genes (DEGs) by defining genes
150 with: i) increased expression upon IFN-λ stimulation in WT mice, ii) decreased expression upon
151 ABX treatment in WT mice, and iii) decreased expression in *Ifnlr1*$^{-/-}$ mice relative to WT mice. The
152 DEGs shared by each of these comparisons comprised a set of 21 genes that are decreased
153 upon treatment with ABX and loss of *Ifnlr1*, and are induced in response to IFN-λ (**Figure 1F**).
154 This set of homeostatic ISGs includes antiviral genes that are dependent on bacterial microbiota
155 and the IFN-λ pathway. Comparison of homeostatic ISG transcript counts between experimental
156 treatments revealed similar insights as prior GSEA analysis. WT mice treated with IFN-λ had
157 higher expression of all homeostatic ISGs than untreated mice, whereas WT mice with a
158 conventional microbiota had higher expression of homeostatic ISGs than *Ifnlr1*$^{-/-}$ mice and ABX-
159 treated mice of both genotypes (**Figure 1G**). We did not detect additional decreases in these
160 homeostatic ISGs in ABX-treated *Ifnlr1*$^{-/-}$ mice relative to conventional *Ifnlr1*$^{-/-}$ mice, suggesting

161 that *Ifnlr1* is necessary for expression of homeostatic ISGs (**Figure 1G**). These results indicate
162 that there is modest but significant expression of ISGs at homeostasis that is lost with *Ifnlr1*
163 deficiency or ABX treatment. Together, these analyses revealed a homeostatic signature of ISGs
164 in the ileum that depends upon the presence of bacterial microbiota and on intact IFN-λ signaling.

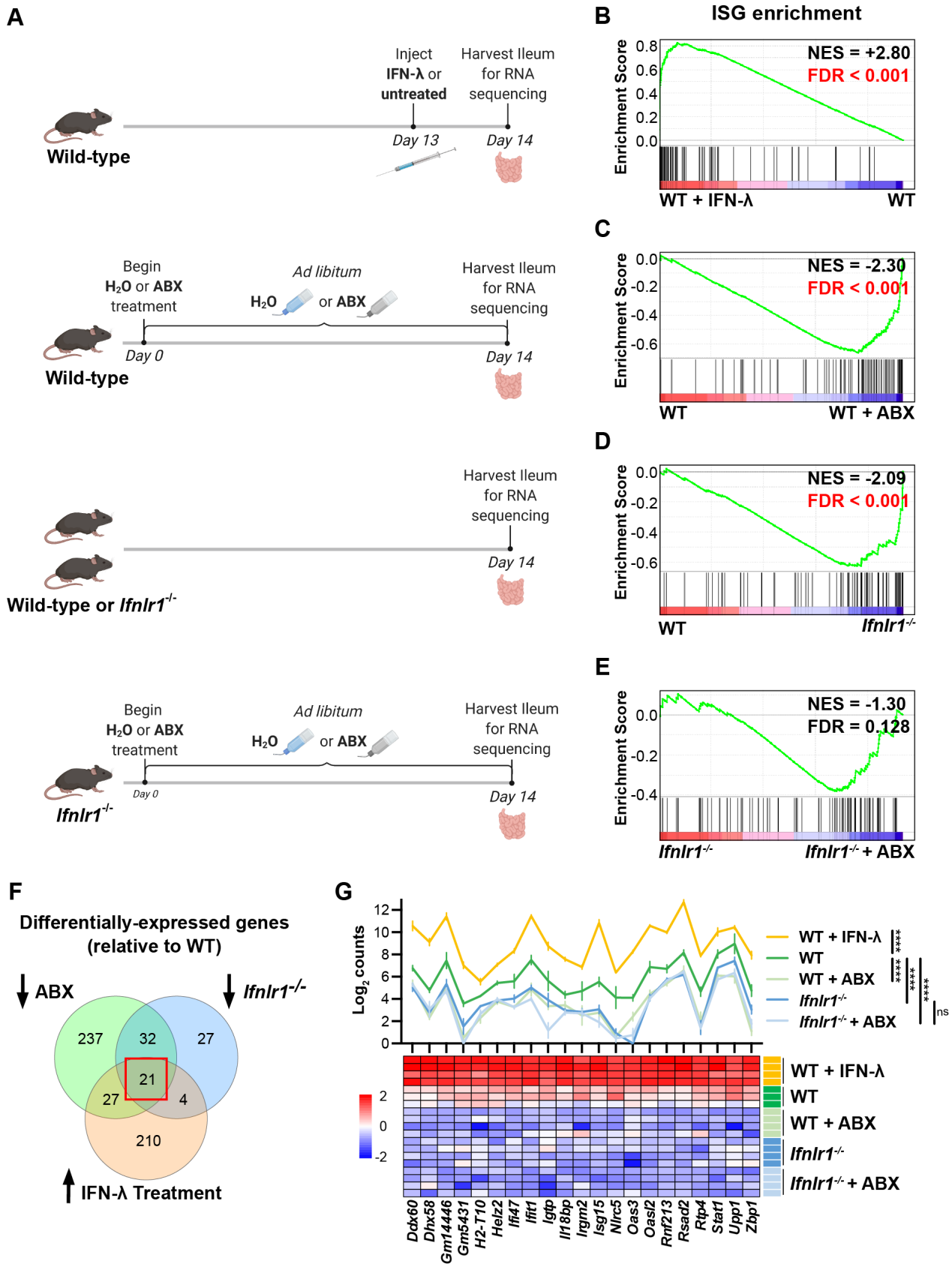
A
Inject IFN-λ or untreated
Harvest Ileum for RNA sequencing
Day 13
Day 14
Wild-type
Begin H2O or ABX treatment
Ad libitum
H2O
or ABX
Harvest Ileum for RNA sequencing
Day 0
Day 14
Wild-type
Harvest Ileum for RNA sequencing
Day 14
Wild-type or Ifnlr1-/-
Begin H2O or ABX treatment
Ad libitum
H2O
or ABX
Harvest Ileum for RNA sequencing
Day 0
Day 14
Ifnlr1-/-
B
ISG enrichment
Enrichment Score
NES = +2.80
FDR < 0.001
WT + IFN-λ
WT
C
Enrichment Score
NES = -2.30
FDR < 0.001
WT
WT + ABX
D
Enrichment Score
NES = -2.09
FDR < 0.001
WT
Ifnlr1-/-
E
Enrichment Score
NES = -1.30
FDR = 0.128
Ifnlr1-/-
Ifnlr1-/- + ABX
F
Differentially-expressed genes (relative to WT)
ABX
Ifnlr1-/-
237
32
27
21
27
4
210
IFN-λ Treatment
G
Log2 counts
WT + IFN-λ
WT
WT + ABX
Ifnlr1-/-
Ifnlr1-/- + ABX
****
****
****
****
****
ns
Ddx60
Dhx58
Gm14446
Gm5431
H2-T10
Helz2
Ifi47
Ifit1
Igtp
Il18bp
Irgm2
Isg15
Nlrc5
Oas3
Oasl2
Rnf213
Rsad2
Rtp4
Stat1
Upp1
Zbp1

166 **Figure 1. Bacterial microbiota stimulate IFN-λ response genes in the ileum at homeostasis.**
167 **A.** Depiction of experimental treatments and comparison groups. Following the indicated
168 treatments, a segment of whole ileum tissue was harvested and analyzed by RNA sequencing for
169 differentially expressed genes between paired conditions. **B-E.** Gene-set enrichment analysis of
170 INTERFERON_ALPHA_RESPONSE hallmark genes (ISGs) was performed with the following
171 comparisons: WT mice treated with 25μg of IFN-λ relative to WT mice treated with PBS **(B)**, WT
172 mice treated with ABX relative to untreated WT mice **(C)**, *Ifnlr1*$^{-/-}$ mice relative to WT mice **(D)**,
173 and *Ifnlr1*$^{-/-}$ mice treated with ABX relative to untreated *Ifnlr1*$^{-/-}$ mice **(E)**. Normalized enrichment
174 score (NES) and false-discovery rate (FDR) are overlaid for each comparison with significant
175 FDR's highlighted (red). **F.** A Venn diagram depicting the total number of differentially expressed
176 genes that are i) increased with IFN-λ stimulation (orange), ii) decreased with ABX treatment
177 (green), or iii) decreased in *Ifnlr1*$^{-/-}$ mice relative to WT (blue). An overlapping subset of 21 genes
178 was shared among all three comparisons (red box). **G.** A graph and heatmap of the relative
179 expression of the 21 genes that overlap in all experimental groups in **(F)** ('homeostatic ISGs').
180 Statistical significance in **(G)** was determined by one-way ANOVA with Tukey's multiple
181 comparisons where ns = $p > 0.05$, and **** = $p < 0.0001$.

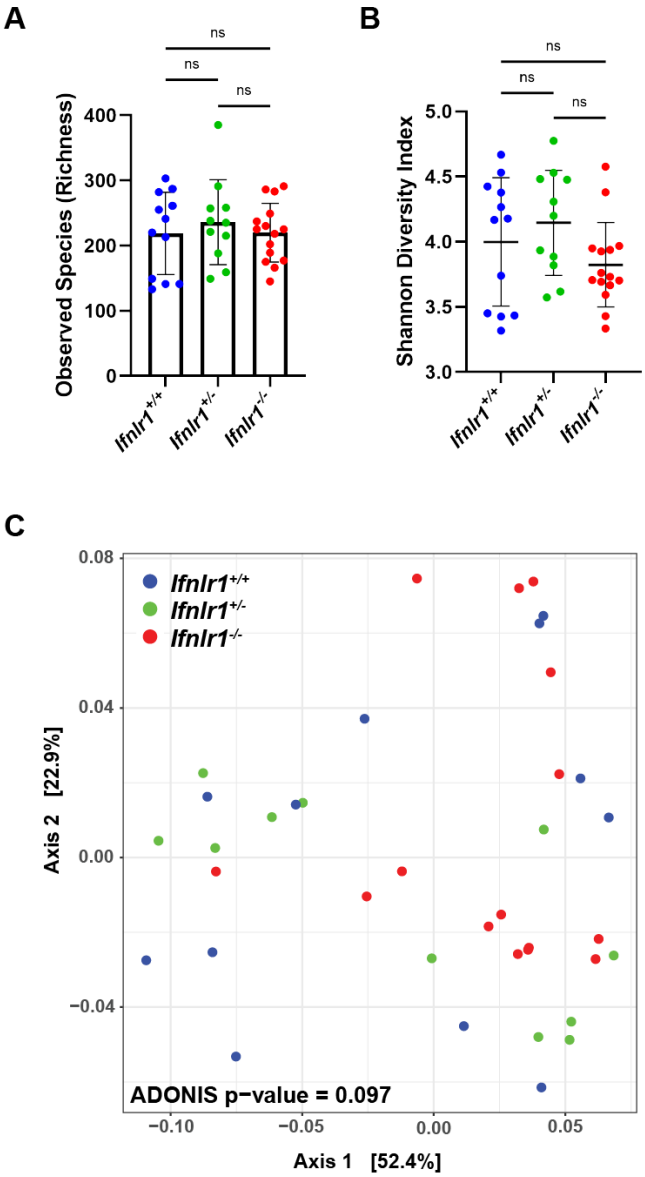

Figure S1. *Ifnlr1*-deficiency does not alter intestinal bacterial microbiota. Stool was harvested from *Ifnlr1*$^{+/+}$, *Ifnlr1*$^{+/-}$, and *Ifnlr1*$^{-/-}$ mice and 16S rRNA genes were sequenced. Alpha-diversity metrics of observed bacterial species **(A)** and Shannon Diversity Index **(B)**. **C.** Principle component analysis of beta-diversity UniFrac distances. Statistical significance was determined one-way ANOVA with Tukey's multiple comparisons, where ns = $p > 0.05$.

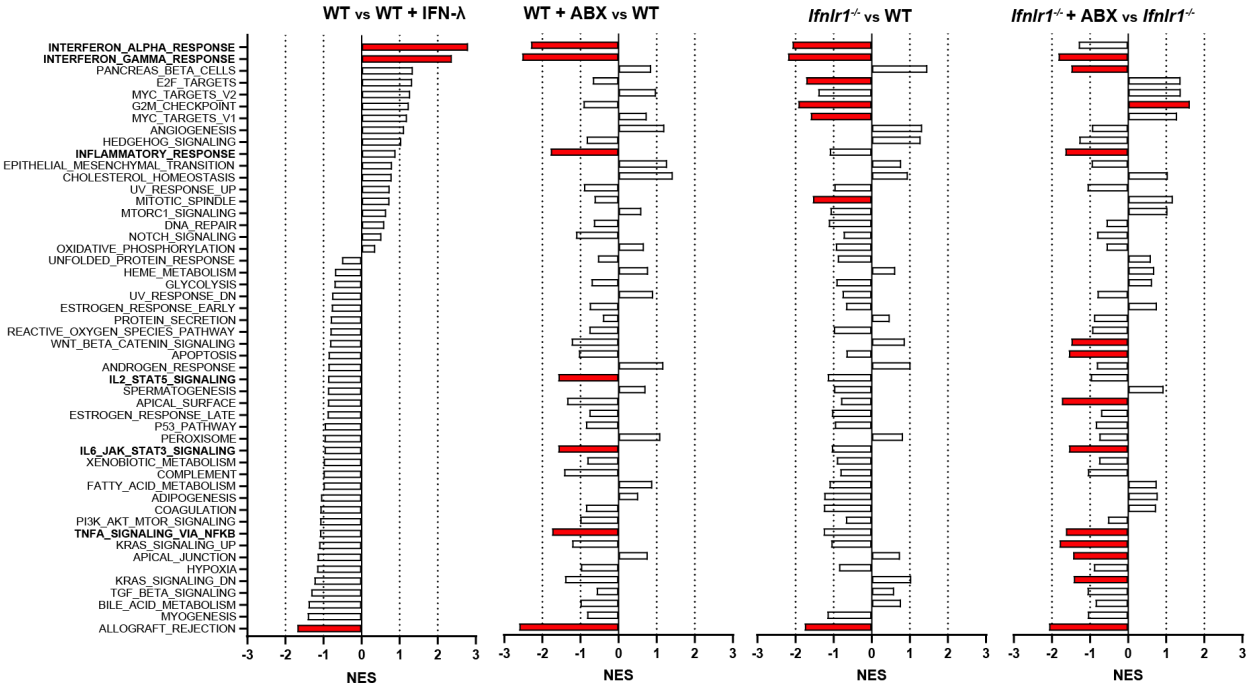

Figure S2. Gene set enrichment analysis of hallmark gene sets. Log_2 counts from RNA sequencing output were assessed for enrichment and depletion of hallmark gene sets by gene set enrichment analysis. Graphs of normalized enrichment score (NES) are displayed for each hallmark gene set and each comparison. Gene sets in red are statistically significantly altered in their given comparison.

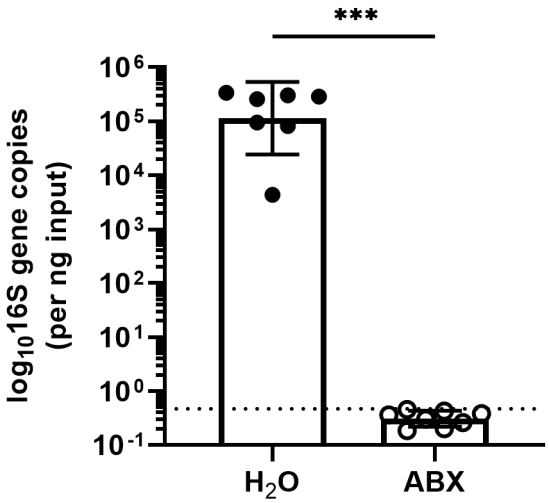

195 **Figure S3. Treatment with antibiotics reduces enteric 16S gene copies to below the limit of**
196 **detection.** rDNA was isolated from luminal contents of mice after 14 days of ABX-treatment. 16S
197 gene copies were assessed by qPCR and normalized to input. Limit of detection: dashed line.
198 Data points represent individual mice and are pooled from 2 independent experiments. Statistical
199 significance was determined by Mann Whitney, where *** = $p < 0.001$.
200

201 **Homeostatic, microbiota- and *Ifnlr1*-dependent ISGs are primarily expressed in intestinal**
202 **tissues**

203 To complement the results of the RNA-sequencing and extend this analysis to other tissue
204 sites**,** we quantified tissue-level expression of a panel of three ISGs by qPCR: *Ifit1, Oas1a*, and
205 *Stat1*. *Ifit1* and *Stat1* were present among the 21 homeostatic ISGs in the preceding analysis and
206 *Oas1a* was included as a representative canonical ISG that we hypothesized would be present in
207 the homeostatic signature, but did not meet the statistical criteria used to define the core set of
208 21 homeostatic ISGs (**Figure 1F-G**). We assessed absolute abundance of these ISG transcripts
209 in the ileum, colon, mesenteric lymph nodes (MLN), and spleen tissue of WT and *Ifnlr1*$^{-/-}$ mice
210 with or without ABX treatment (**Figures 2A-C**). Consistent with our RNA-seq data, these ISGs
211 were reduced in the ilea of *Ifnlr1*$^{-/-}$ mice and ABX-treated WT mice compared to WT mice with
212 conventional microbiota (**Figure 2A**). Secondly, homeostatic ISGs were expressed in WT colonic
213 tissue and were significantly decreased in colonic tissue of *Ifnlr1*$^{-/-}$ mice and ABX-treated WT mice
214 (**Figure 2B**). These data indicate that homeostatic ISGs in both the ileum and colon were
215 dependent on *Ifnlr1* and the bacterial microbiota; however, these homeostatic ISGs were more
216 abundantly expressed in ileal tissue than colonic tissue (**Figure S4**). To confirm that treatment
217 with ABX does not ablate the ability of the intestine to respond to IFN-λ, we stimulated ABX-
218 treated mice with intraperitoneal IFN-λ and harvested ileum tissue. Stimulation with small amounts
219 of IFN-λ rescued ISG expression in whole tissue (**Figure S5**), indicating that that reduction of

220 homeostatic ISG expression upon treatment with ABX is not due to an inability of the intestine to
221 respond to IFN-λ.

222 Enteric colonization by bacteria was shown to stimulate systemic type I IFN responses
223 (Abt et al., 2012; Bradley et al., 2019; Ganal et al., 2012; Steed et al., 2017; Stefan et al., 2020;
224 Winkler et al., 2020), so we assessed whether the decreases in ISGs upon ABX treatment or loss
225 of *Ifnlr1* in the ileum were recapitulated in systemic immune tissues. We quantified *Ifit1*, *Stat1,*
226 and *Oas1a* expression in the MLN and the spleen and found that ABX treatment and *Ifnlr1* deletion
227 did not reduce ISGs in these tissues (**Figure 2C**). Although we observe increases in *Ifit1*
228 expression in MLN upon treatment with ABX, these results are not recapitulated by *Stat1* and
229 *Oas1a* expression, and no significant changes in ISG expression were detected in the spleen.
230 Cumulatively, these data indicate that homeostatic ISGs include genes beyond the core signature
231 identified in **Figure 1** (e.g. *Oas1a*), that homeostatic ISGs are present in colonic tissue, and that
232 homeostatic IFN-λ stimulated genes are most prominent in enteric tissues.

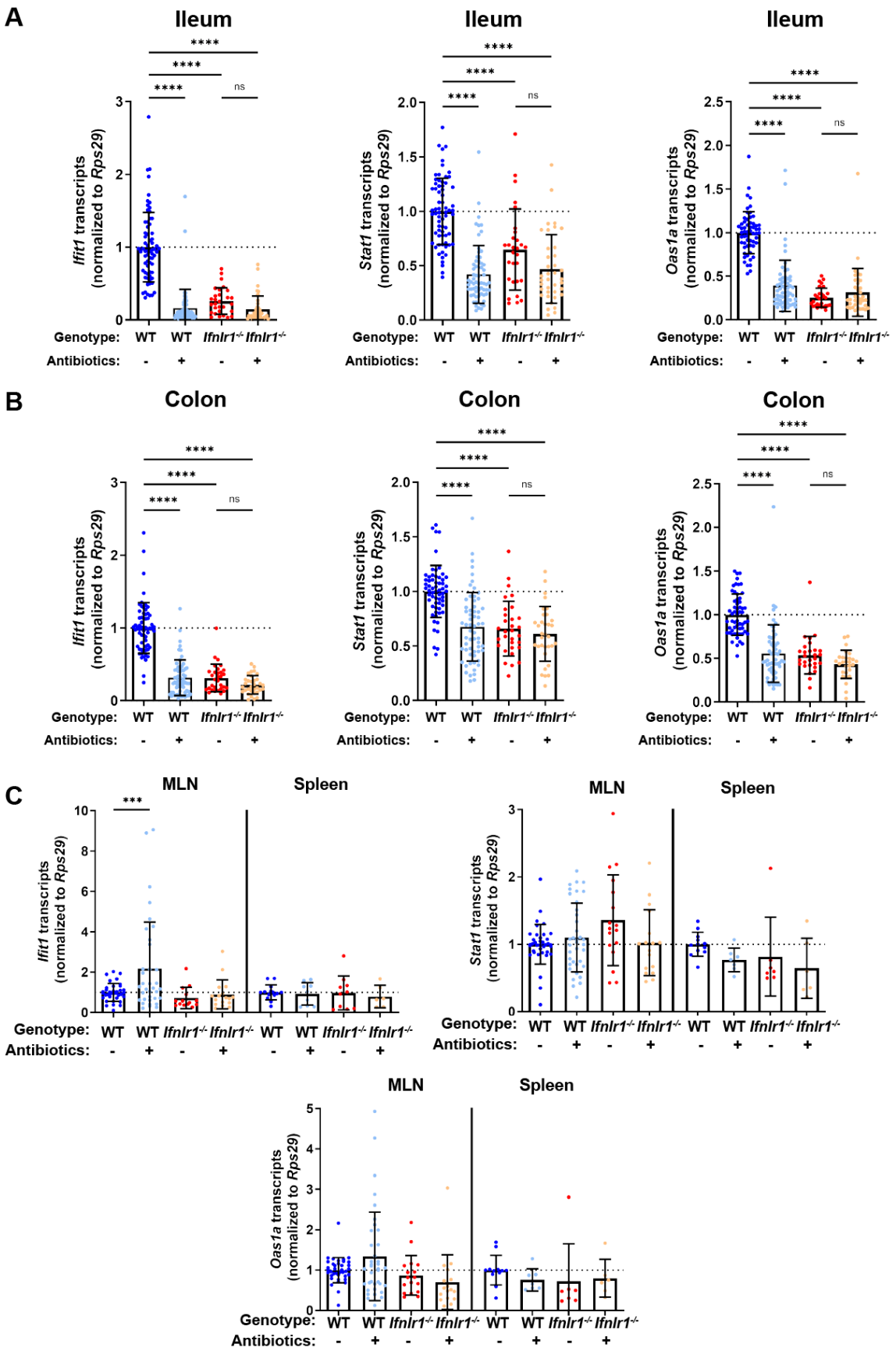
A
Ileum
Ileum
Ileum
Ifit1 transcripts (normalized to Rps29)
Stat1 transcripts (normalized to Rps29)
Oas1a transcripts (normalized to Rps29)
****
ns
Genotype: WT WT Ifnlr1-/- Ifnlr1-/-
Antibiotics: - + - +
B
Colon
Colon
Colon
C
MLN
Spleen
***

233

Figure 2. Homeostatic, microbiota- and *Ifnlr1*-dependent ISGs are primarily expressed in intestinal tissues. A segment of ileum or colon tissue from WT or *Ifnlr1*$^{-/-}$ mice was harvested following H_2O or ABX treatment and the ISGs *Ifit1*, *Stat1*, and *Oas1a* were analyzed by qPCR. Transcripts were quantified in ileum **(A)**, colon **(B),** or MLN and spleen **(C)** with normalization to untreated WT mice. Data points represent individual mice and data are pooled from 10-20 independent experiments in **A-B** and 15 independent experiments in **C**. Statistical significance was determined by one-way ANOVA with Tukey's multiple comparisons in **A-B** and Dunnett's multiple comparisons in **C**. * = p < 0.05, ** = p < 0.01, *** = p < 0.001, **** = p < 0.0001.

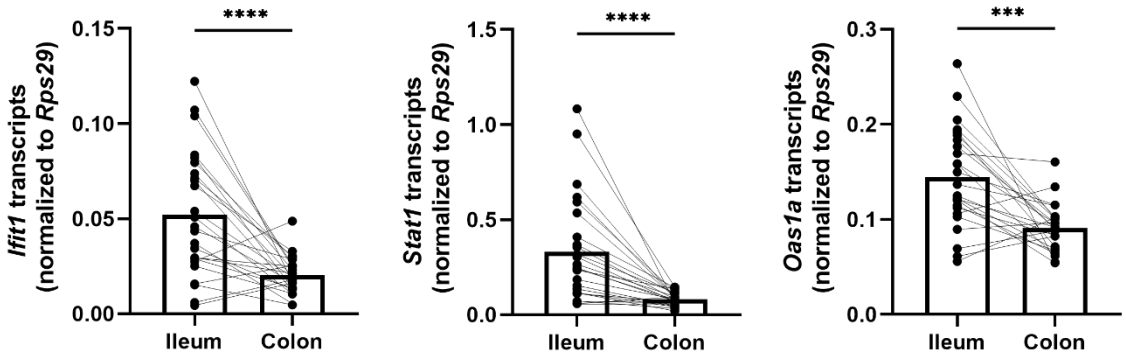

Figure S4. Homeostatic ISGs are more abundantly expressed in the ileum than in the colon. *Ifit1*, *Stat1*, and *Oas1a* expression was quantified from the ileum and colon tissue of WT mice. Data points represent individual mice and are pooled from 5 independent experiments. Statistical significance was determined by paired t-test where *** = p < 0.001 and **** = p < 0.0001.

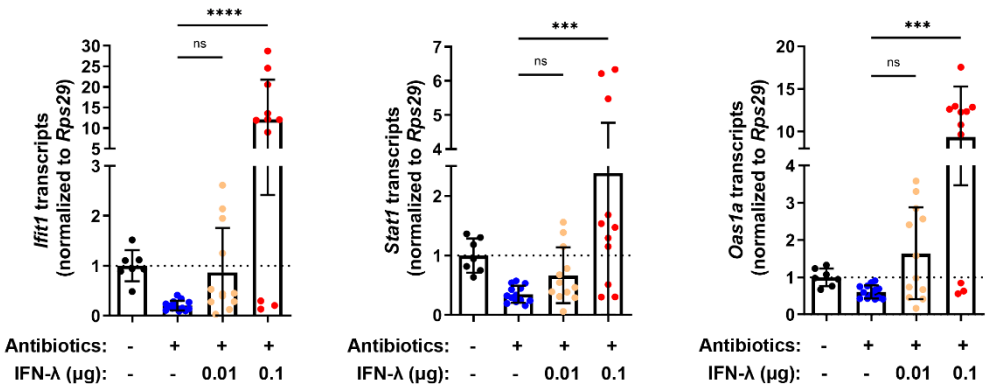

248 **Figure S5. Treatment with antibiotics does not ablate responsiveness to IFN-λ.** *Ifit1*, *Stat1*,
249 and *Oas1a* expression was quantified in the ileum of WT mice treated with or without ABX and
250 was normalized to untreated mice. Increasing quantities of IFN-λ were intraperitoneally injected
251 into ABX-treated mice to rescue basal ISG expression. Data points represent individual mice and
252 are pooled from 3 independent experiments. Statistical significance was determined by Kruskal-
253 Wallis test with Dunn's multiple comparisons with *** = $p < 0.001$, and **** = $p < 0.0001$.
254

255 **Homeostatic ISG expression in the intestine is independent of type I IFN**

256 To determine whether detection of enteric bacteria by TLRs stimulates homeostatic ISGs,
257 we measured tissue ISG expression in mice that were deficient in TRIF or MYD88. Signaling
258 through TRIF results in activation of interferon regulatory factors (IRFs), such as IRF3 and IRF7,
259 that commonly contribute to IFN induction (Honda et al., 2005a; Osterlund et al., 2007; Schmid et
260 al., 2010). Additionally, signaling through MYD88 can aid initiation of IFN expression, through
261 nuclear factor kappa-light-chain-enhancer of activated B cells (NF-κB) transcription factor family
262 members (Osterlund et al., 2007) and IRF7 (Honda et al., 2005b; Tomasello et al., 2018). *Ifit1*
263 expression in the ileum and colon of *Trif*$^{-/-}$ mice was not significantly different than in WT mice,
264 and *Ifit1* expression was reduced with ABX in *Trif*$^{-/-}$ mice (**Figure 3A**). However, we found that
265 mice lacking *Myd88* exhibited tissue-specific decreases in *Ifit1* expression, with significant
266 decreases in the ileum, but not in the colon, relative to WT mice (**Figure 3A)**. These data are
267 consistent with a previous report (Stockinger et al., 2014) and suggest that signaling through
268 MYD88, but not TRIF, is necessary for homeostatic ISG expression in the ileum, whereas other
269 factors may dominate in the colon.

270 To expand these findings, we assessed the role of IRF3 and IRF7 transcription factors
271 that are commonly activated downstream of MYD88 and TRIF. We did not observe significant
272 decreases in *Ifit1* expression in the ileum or the colon of *Irf3*$^{-/-}$ mice as compared to WT (**Figure**
273 **3B**), indicating that IRF3 is not required for homeostatic IFN-λ induction. However, we observed

274 a modest (two-fold) decrease in *Ifit1* expression in both the ileum and colon of *Irf7*$^{-/-}$ mice when
275 compared to WT mice (**Figure 3B**). Although IRF7 is implicated by these data, it does not appear
276 to be strictly required for homeostatic expression of *Ifit1* because expression is further reduced
277 by ABX treatment (**Figure 3B**). These data suggest that IRF7 is not necessary for the homeostatic
278 ISG response to the bacterial microbiota.

279 Type I and III IFNs stimulate overlapping ISG responses that are both dependent on
280 STAT1. Therefore, to further investigate the contribution of type I IFN signaling to homeostatic
281 ISG expression, we quantified *Ifit1* expression in ileum and colon tissue from *Ifnar1*$^{-/-}$ or *Stat1*$^{-/-}$
282 mice. *Ifit1* expression was not significantly different in either ileum or colon tissue of *Ifnar1*$^{-/-}$ mice
283 compared to WT (**Figure 3C**). However, *Ifit1* expression was significantly lower in ileum and colon
284 tissue of *Stat1*$^{-/-}$ mice compared to *Ifnar1*$^{-/-}$ and WT mice. Importantly, treatment of *Stat1*$^{-/-}$ mice
285 with ABX did not further reduce *Ifit1* expression, emphasizing the necessity of STAT1 for this
286 homeostatic ISG response.

287 Lastly, to determine whether type I IFN signaling plays a compensatory role in homeostatic
288 ISG expression in the absence of *Ifnlr1*, we bred mice with heterozygous expression of both *Ifnlr1*
289 and *Ifnar1* (*Ifnlr1*^{Het}/*Ifnar1*^{Het}) with mice that lack *Ifnlr1* and *Ifnar1* (*Ifnlr1*^{KO}/*Ifnar1*^{KO}). This breeding
290 scheme produced littermate-matched mice that were *Ifnlr1*^{Het}/*Ifnar1*^{Het}, *Ifnlr1*^{KO}/*Ifnar1*^{KO}, and mice
291 singly deficient in *Ifnlr1* (*Ifnlr1*^{KO}/*Ifnar1*^{Het}) or *Ifnar1* (*Ifnlr1*^{Het}/*Ifnar1*^{KO}). We found that *Ifit1*
292 expression was not significantly different in *Ifnlr1*^{Het}/*Ifnar1*^{KO} relative to *Ifnlr1*^{Het}/*Ifnar1*^{Het} controls
293 in ileal tissue (**Figure 3D**). *Ifit1* expression in *Ifnlr1*^{KO}/*Ifnar1*^{Het} was significantly lower compared to
294 *Ifnlr1*^{Het}/*Ifnar1*^{Het} controls, but was not significantly different from *Ifnlr1*^{KO}/*Ifnar1*^{KO} mice (**Figure**
295 **3D**). Cumulatively, these data indicate that homeostatic ISG expression in the intestine is partly
296 dependent on MYD88, and is independent of type I IFN signaling.

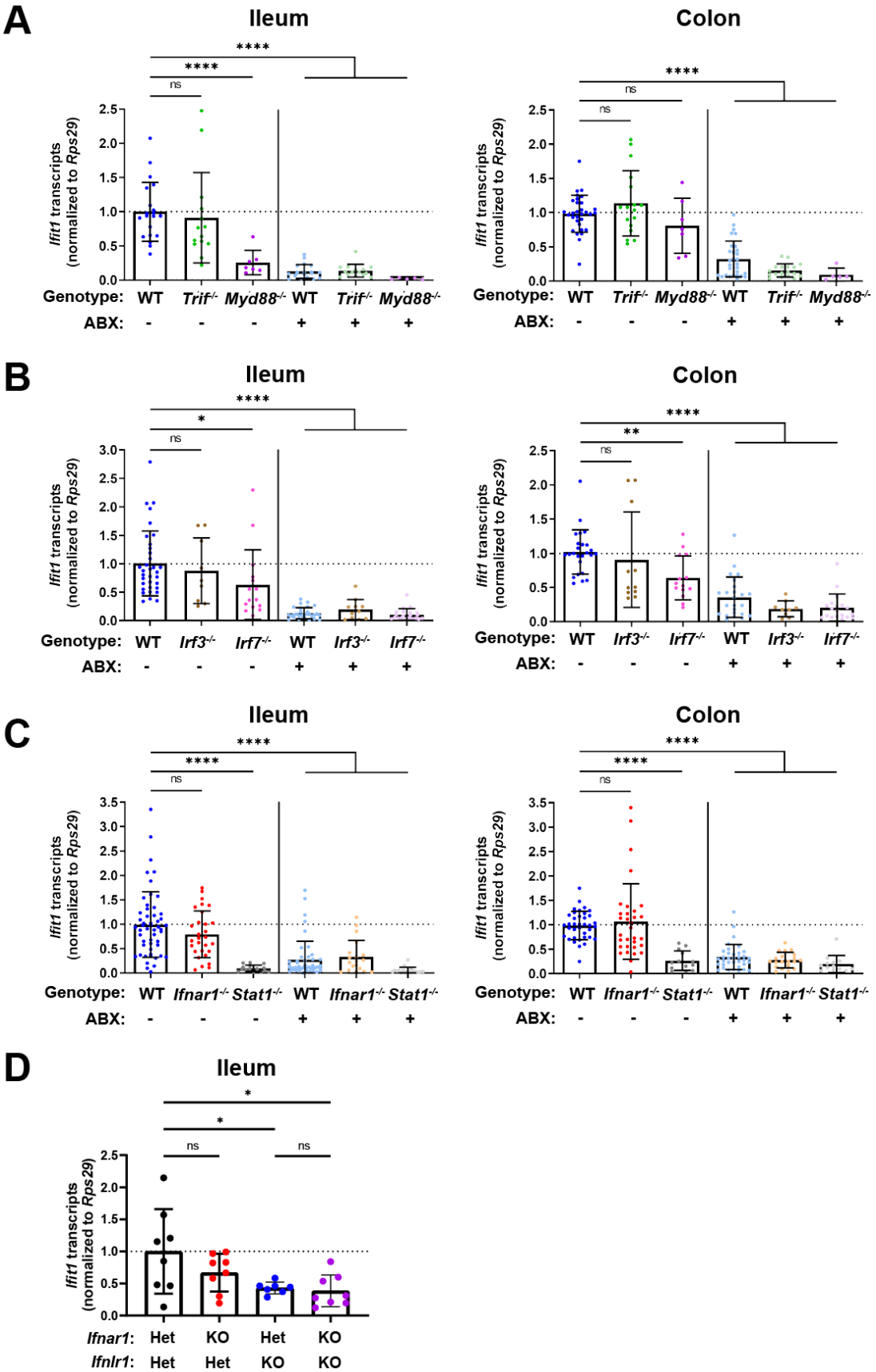
A
Ileum
Colon
Ifit1 transcripts (normalized to Rps29)
Genotype: WT Trif-/- Myd88-/- WT Trif-/- Myd88-/-
ABX: - - - + + +
B
Ileum
Colon
Genotype: WT Irf3-/- Irf7-/- WT Irf3-/- Irf7-/-
ABX: - - - + + +
C
Ileum
Colon
Genotype: WT Ifnar1-/- Stat1-/- WT Ifnar1-/- Stat1-/-
ABX: - - - + + +
D
Ileum
Ifnar1: Het KO Het KO
Ifnlr1: Het Het KO KO

297

298 **Figure 3. Homeostatic ISG expression is independent of type I IFN.** *Ifit1* expression levels
299 were assessed by qPCR from the ileum or colon of **(A)** *Trif*$^{-/-}$ and *Myd88*$^{-/-}$, **(B)** *Irf3*$^{-/-}$ *and Irf7*$^{-/-}$, or
300 **(C)** *Ifnar1*$^{-/-}$ and *Stat1*$^{-/-}$ mice treated with or without ABX normalized to untreated, WT mice. Some
301 WT controls are shared across experiments in **(A-C). D.** *Ifit1* expression was measured by qPCR
302 in ileum tissue of indicated genotypes. Data points represent individual mice and are pooled from
303 at least six independent experiments in **(A-C)** and two independent experiments in **(D)**. Statistical
304 significance was determined by one-way ANOVA with Dunnett's multiple comparisons in **(A-C)**
305 and one-way ANOVA with Tukey's multiple comparisons in D, where * = $p < 0.05$, ** = $p < 0.01$,
306 *** = $p < 0.001$, **** = $p < 0.0001$.
307

308 **Homeostatic ISG expression in the intestine is restricted to epithelial cells**

309 Given the primarily epithelial expression of *Ifnlr1*, we assessed which compartment of the
310 ileum expresses homeostatic ISGs by isolating a stripped intestinal epithelial fraction and
311 digesting the underlying lamina propria. We assessed ISG expression in these two fractions from
312 WT and *Ifnlr1*$^{-/-}$ mice treated with or without ABX. Treatment with ABX or loss of *Ifnlr1* reduced
313 homeostatic ISGs in the IEC fraction, but the lamina propria had low expression of these ISGs
314 relative to the epithelium of untreated WT mice, regardless of treatment or genotype (**Figure 4A**).

315 IECs express abundant *Ifnlr1*, but other intra-epithelial cell types do not (Mahlakõiv et al.,
316 2015; Sommereyns et al., 2008). To determine whether *Ifnlr1* expression by IECs was required
317 for homeostatic ISG expression, we used mice with IECs that are conditionally deficient in *Ifnlr1*
318 (*Ifnlr1*$^{\Delta IEC}$) and littermates that retain normal *Ifnlr1* expression (*Ifnlr1*$^{flox/flox}$) (Baldridge et al., 2017).
319 *Ifit1* and *Oas1a* expression in the ileum (**Figure 4B**) and colon (**Figure 4C**) of *Ifnlr1*$^{flox/flox}$ mice was
320 decreased upon treatment with ABX, consistent with the phenotype observed in WT mice.
321 Conditional deletion of *Ifnlr1* in IECs reduced *Ifit1* and *Oas1a* to a similar extent as the reduction
322 observed in *Ifnlr1*$^{-/-}$ animals, above (**Figures 2A-B**). Together, these findings indicate that
323 homeostatic ISGs are dependent on *Ifnlr1*-expression by IECs.

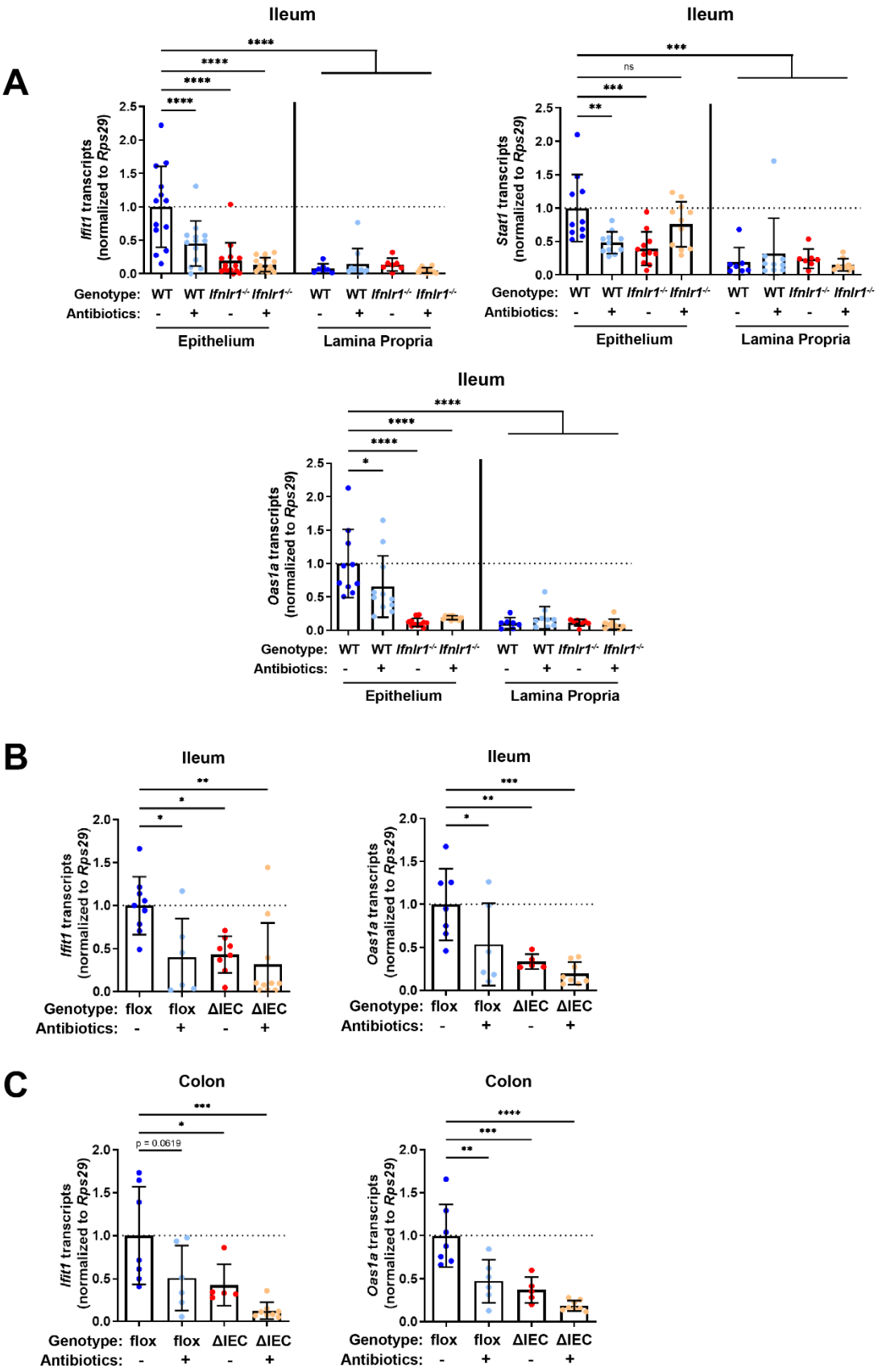
A
Ileum
Ifit1 transcripts (normalized to Rps29)
Genotype: WT WT Ifnlr1-/- Ifnlr1-/- WT WT Ifnlr1-/- Ifnlr1-/-
Antibiotics: - + - + - + - +
Epithelium
Lamina Propria
Ileum
Stat1 transcripts (normalized to Rps29)
ns
Ileum
Oas1a transcripts (normalized to Rps29)
B
Ileum
Ifit1 transcripts (normalized to Rps29)
Genotype: flox flox ΔIEC ΔIEC
Antibiotics: - + - +
Ileum
Oas1a transcripts (normalized to Rps29)
C
Colon
p = 0.0619
Colon

324

325 **Figure 4. Homeostatic ISG expression in the intestine is restricted to epithelial cells**. **A.**
326 *Ifit1*, *Stat1*, and *Oas1a* expression was quantified in stripped epithelial cells or in the lamina
327 propria cells of the ileum. Comparisons were performed between WT and *Ifnlr1*$^{-/-}$ mice with or
328 without ABX treatment, and ISG expression was normalized to WT values. **B-C.** *Ifit1* and *Oas1a*
329 expression from the **(B)** ileum or **(C)** colon of mice with conditional presence (flox) or absence
330 (ΔIEC) of *Ifnlr1* in intestinal epithelial cells. Data points represent individual mice and are pooled
331 from three independent experiments in **(A)** and two independent experiments in **(B-C)**. Statistical
332 significance was determined by one-way ANOVA with Dunnett's multiple comparisons. * = $p < 0.05$, ** = $p < 0.01$, *** = $p < 0.001$.
333
334

335 **Bacterial microbiota stimulate expression of *Ifnl2/3* by CD45-positive cells**

336 A previous study (Mahlakõiv et al., 2015) noted the presence of IFN-λ transcripts (*Ifnl2/3*)
337 at homeostasis in CD45+ cells within the stripped intestinal epithelium, but not in the lamina
338 propria. To extend these findings and to determine whether CD45+ cells in the intestinal
339 epithelium produce IFN-λ in response to bacterial microbiota at homeostasis, we enriched cell
340 subsets from epithelial or lamina propria fractions of the ileum for quantification of *Ifnl2/3* by qPCR.
341 We treated WT mice with control, ABX, or stimulation with a synthetic dsRNA analogue (poly I:C).
342 We then magnet-enriched EpCAM+ or CD45+ cells from stripped intestinal epithelium or digested
343 lamina propria ileal tissue (**Figure S6**). We found that CD45+ cells from the intestinal epithelial
344 and lamina propria fraction expressed detectable *Ifnl2/3* at homeostasis, but EpCAM+ cells did
345 not, which is consistent with Mahlakõiv et al. Furthermore, we found that expression of *Ifnl2/3* in
346 CD45+ cells from the epithelial fraction was significantly reduced with ABX-treatment, and CD45+
347 cells from lamina propria had a non-statistically-significant ($p = 0.0523$) reduction in *Ifnl2/3*
348 expression with ABX-treatment (**Figure 5A**). From these data, we conclude that epithelium-
349 associated CD45+ leukocytes are the likely source of homeostatic IFN-λ in response to bacterial
350 microbiota, but we do not rule out additional involvement of CD45+ cells in the lamina propria.

351 Similar to *Ifnl2/3*, we found that CD45+ cells of the epithelial fraction modestly expressed
352 IFN-β transcript (*Ifnb1*) at homeostasis. Additionally, CD45+ cells of the lamina propria robustly
353 expressed *Ifnb1* at homeostasis. However, unlike *Ifnl2/3*, *Ifnb1* was not decreased in mice treated
354 with ABX (**Figure 5B**). These data indicate that *Ifnb1* expression by CD45+ cells in the intestine
355 is less dependent on stimulation by bacterial microbiota relative to *Ifnl2/3*, consistent with the
356 dominant role of IFN-λ responses in driving homeostatic ISG expression in the epithelium.

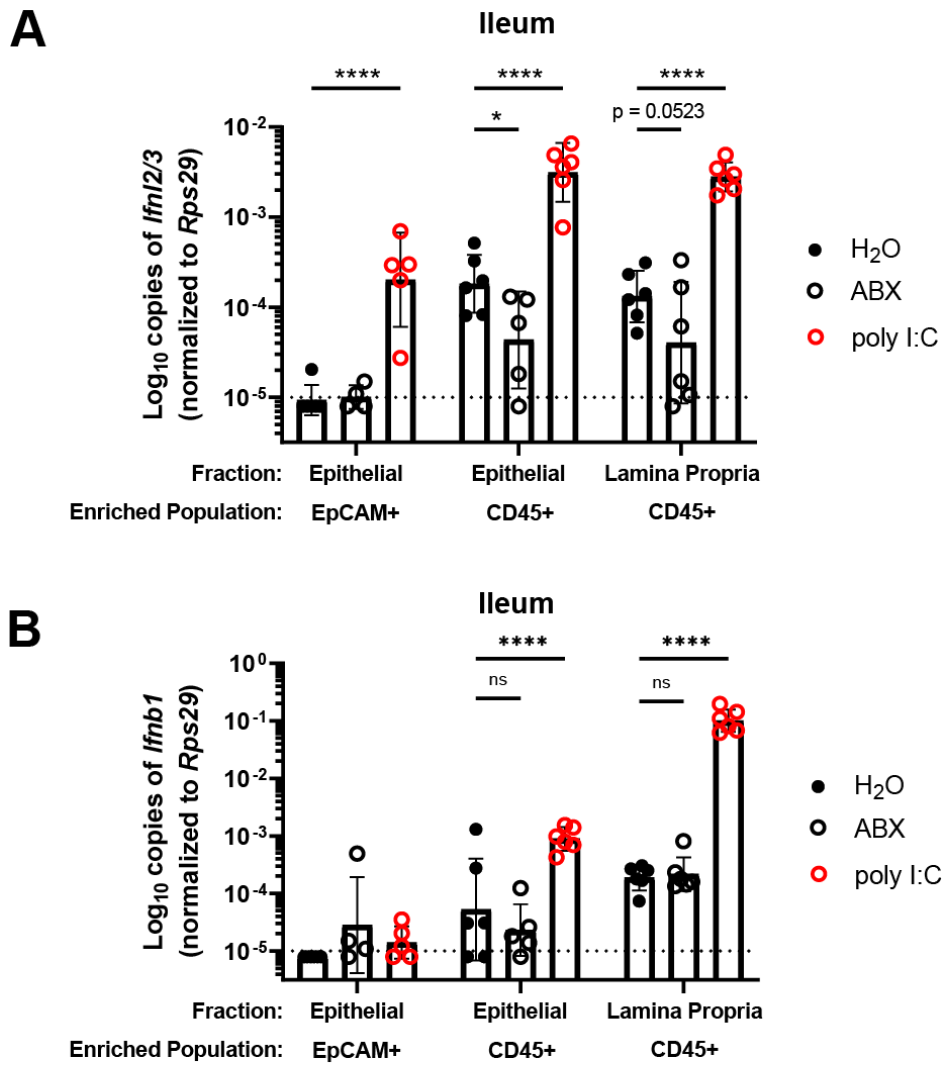

357

358 **Figure 5. Bacterial microbiota stimulate expression of *Ifnl2/3* by CD45-positive cells. A-B.**
359 Cellular suspensions from the ileal epithelium and lamina propria was harvested from WT mice
360 treated with H_2O, ABX, or stimulated with poly I:C. Resulting cells were enriched for EpCAM-

361 positive and CD45-positive cells by magnetic separation. *Ifnl2/3* expression **(A)** and *Ifnb1*
362 expression **(B)** was quantified from each enriched cellular fraction by qPCR. Data points represent
363 individual mice and are pooled from 2 independent experiments. Statistical significance was
364 determined by two-way ANOVA with Dunnett's multiple comparisons, where * = $p < 0.05$ and ****
365 = $p < 0.0001$.

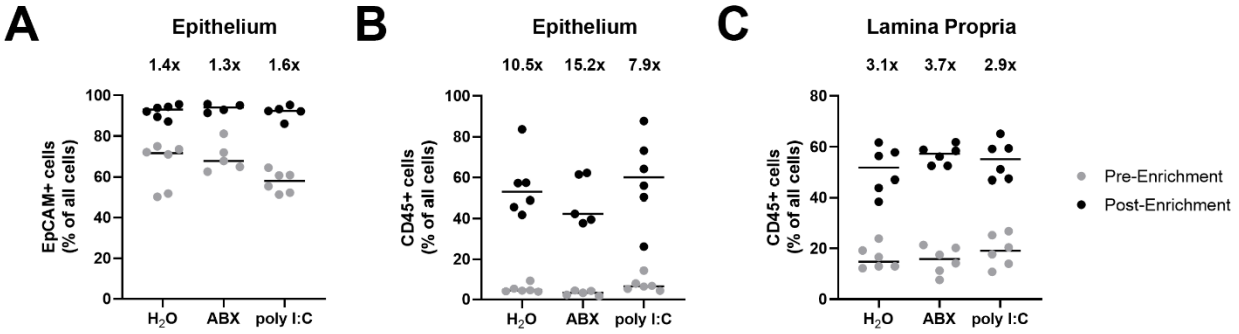

366

367 **Figure S6. Enrichment of EpCAM+ and CD45+ cells from the intestinal epithelium and**
368 **lamina propria. A-C.** The ileal epithelium and lamina propria was harvested from WT mice
369 treated with H_2O, ABX, or stimulated with poly I:C. Resulting cell suspensions were enriched for
370 EpCAM-positive and CD45-positive cells and the purity of all live and dead cells pre- and post-
371 enrichment were quantified by flow cytometry. The percentage of live and dead cell events with
372 surface expression of **(A)** EpCAM or **(B)** CD45 prior to- and following- enrichment from stripped
373 intestinal epithelium. **C.** The percentage of live and dead cell events with surface expression of
374 CD45 prior to and following CD45 enrichment from isolated lamina propria. Mean fold enrichment
375 for each condition is noted above each column. Data points represent individual mice and are
376 pooled from 2 independent experiments.

377

378 **Homeostatic ISG expression in the small intestine is highly localized**

379 Homeostatic ISG expression in the ileum was of relatively low magnitude when compared
380 to IFN-λ treatment (**Figures 1-2**). Therefore, we hypothesized that a low abundance of
381 homeostatic ISG expression would be uniformly distributed between IECs of the intestinal

382 epithelium, and we sought to assess the distribution of the homeostatic ISG, *Ifit1*, using *in situ*
383 hybridization (RNAscope). Contrary to our hypothesis, RNAscope staining of the ileum from
384 untreated WT mice revealed localized pockets of robust *Ifit1* expression in individual villi rather
385 than ubiquitously low expression throughout the intestinal epithelium (**Figure 6A**). Additionally,
386 *Ifit1* localization was skewed away from the crypt and towards the tips of individual villi within the
387 ileum, and this localization was not specific to *Ifit1* because the distinct ISG *Usp18* co-localized
388 with *Ifit1* (**Figure 6A**). These data indicate that homeostatic ISGs are sporadically expressed in
389 individual villi and are primarily localized to mature enterocytes that are most distally located in
390 villi. We determined that localized ISG expression within individual villi was not due to a localized
391 ability to respond to IFN-λ because stimulation with exogenous IFN-λ resulted in *Ifit1* expression
392 within all intestinal villi, but not intestinal crypts (**Figure S7**). The minimal expression of *Ifit1* within
393 intestinal crypts following exogenous IFN-λ treatment suggests that homeostatic ISGs are
394 localized to mature enterocytes because intestinal crypts do not exhibit robust responses to IFN-
395 λ. Additionally, the non-uniform distribution of homeostatic *Ifit1* expression was ablated in the
396 ileum of mice treated with ABX (**Figures 6B-D**), consistent with a dependency on bacterial
397 microbiota. To determine whether localized *Ifit1* expression was dependent on IEC expression of
398 *Ifnlr1*, we assessed the distribution of *Ifit1* expression in the ilea of littermate *Ifnlr1*$^{flox/flox}$ and
399 *Ifnlr1*$^{\Delta IEC}$ mice. We found that the localized *Ifit1* expression observed in untreated WT mice was
400 recapitulated in *Ifnlr1*$^{flox/flox}$ mice (**Figure 6E**), but these areas of ISG expression were ablated in
401 *Ifnlr1*$^{\Delta IEC}$ mice (**Figures 6F-G**). Lastly, we found that this discrete localization of the homeostatic
402 ISG response is not limited to the ileum, as localized *Ifit1* staining is also observed in the colonic
403 epithelium (**Figure S8**). Together, our analyses indicated that homeostatic ISGs are expressed in
404 a highly localized manner within the intestinal epithelium.

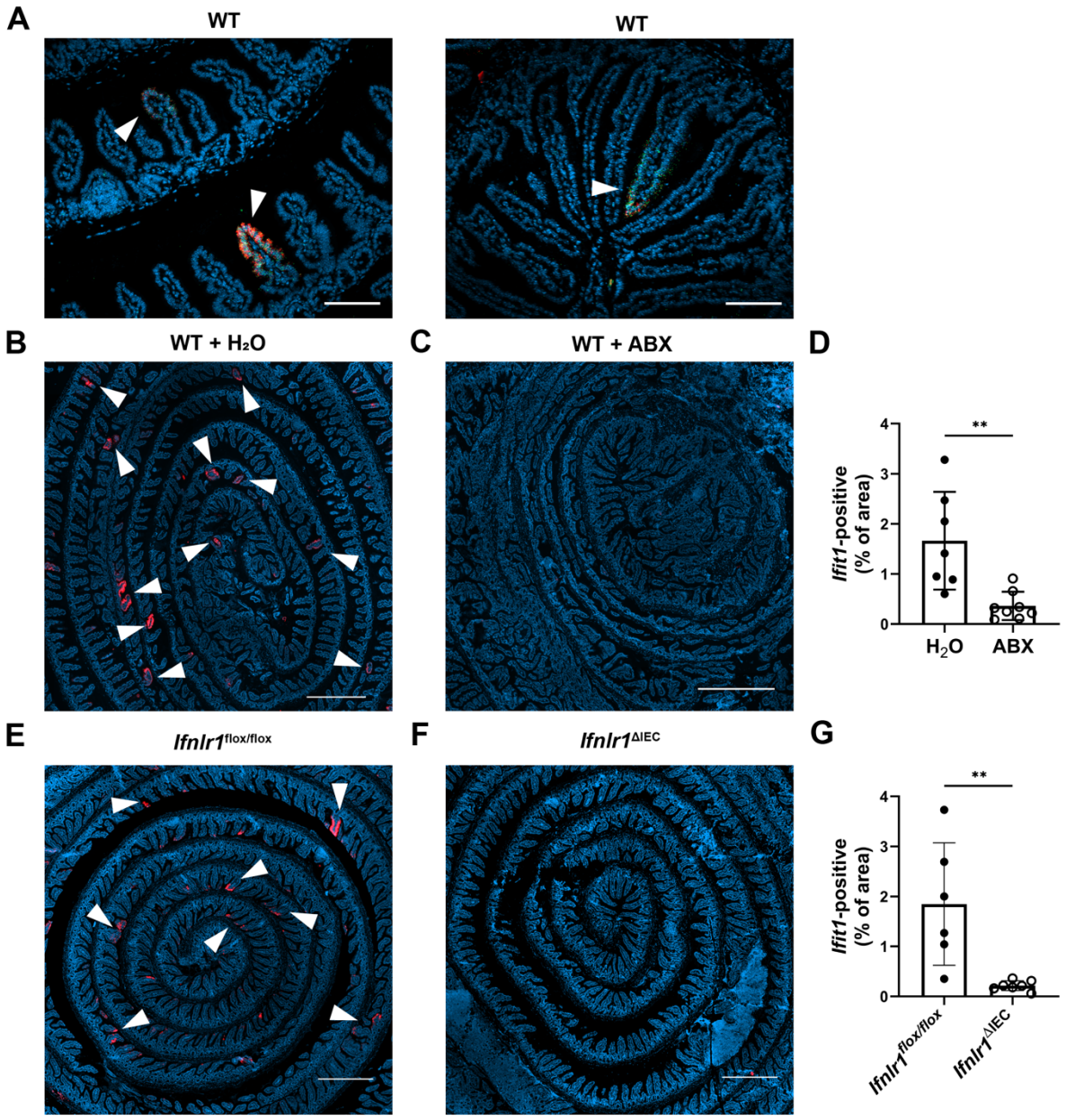

405

406 **Figure 6. Homeostatic ISG expression in the small intestine is highly localized**. The ilea of
407 WT, *Ifnlr1*$^{flox/flox}$, or *Ifnlr1*$^{\Delta IEC}$ mice were harvested, processed into a Swiss rolls, and stained by *in*
408 *situ* hybridization for the ISGs, *Ifit1* (red) and *Usp18* (green), with a DAPI (blue) counterstain. **A.**
409 Representative high-magnification images of co-localized *Ifit1* (red) and *Usp18* (green)
410 expression in the ileum of WT mice, see arrows. **B-D.** WT mice treated with H_2O control or ABX
411 with quantification of *Ifit1* area relative to the total area of the section across replicate mice. **E-G.**
412 *Ifnlr1*$^{flox/flox}$ or *Ifnlr1*$^{\Delta IEC}$ mice at homeostasis with quantification of *Ifit1* area relative to the total area

of the section across replicate mice. Scale bar = 100μm in **(A)** and 500μm in **(B-G)** and. Statistical significance was calculated by unpaired t-test where ** = p < 0.01. Each data point in **(D)** and **(G)** represents an individual mouse from 2 independent experiments.

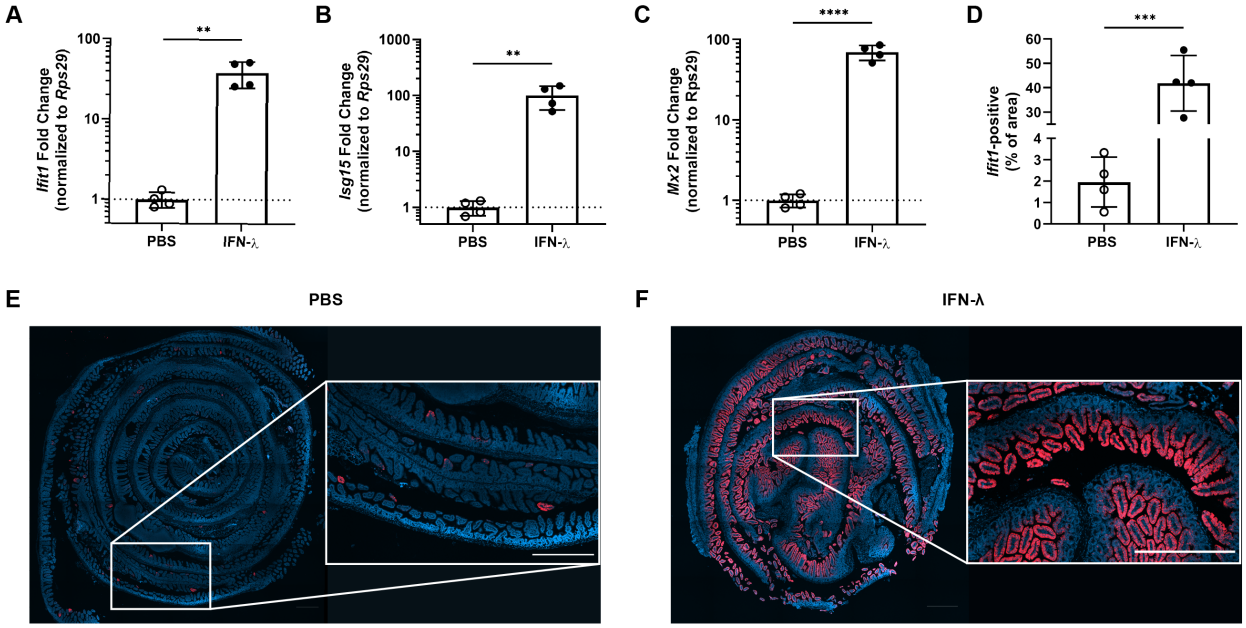

Figure S7. The entire intestinal epithelium is responsive to IFN-λ. Wild-type mice were injected with PBS or 3μg of pegylated IFN-λ3. The ileum was harvested after four hours and a small section was assessed for expression of the ISGs: *Ifit1* **(A)**, *Isg15* **(B)**, and *Mx2* **(C)** by qPCR. The remaining tissue was stained by RNAscope for the ISG, *Ifit1* (red), with a DAPI (blue) counterstain. **D.** Quantification of *Ifit1* area relative to the total area of the section across replicate mice. **E-F.** Representative images from the ileum of mice injected with PBS **(E)** or IFN-λ **(F).** Scale bar = 500μm in insets. Data points represent individual mice from a single experiment. Statistical significance was determined by unpaired t-test with ** = p < 0.01, *** = p < 0.001, and **** = p < 0.0001.

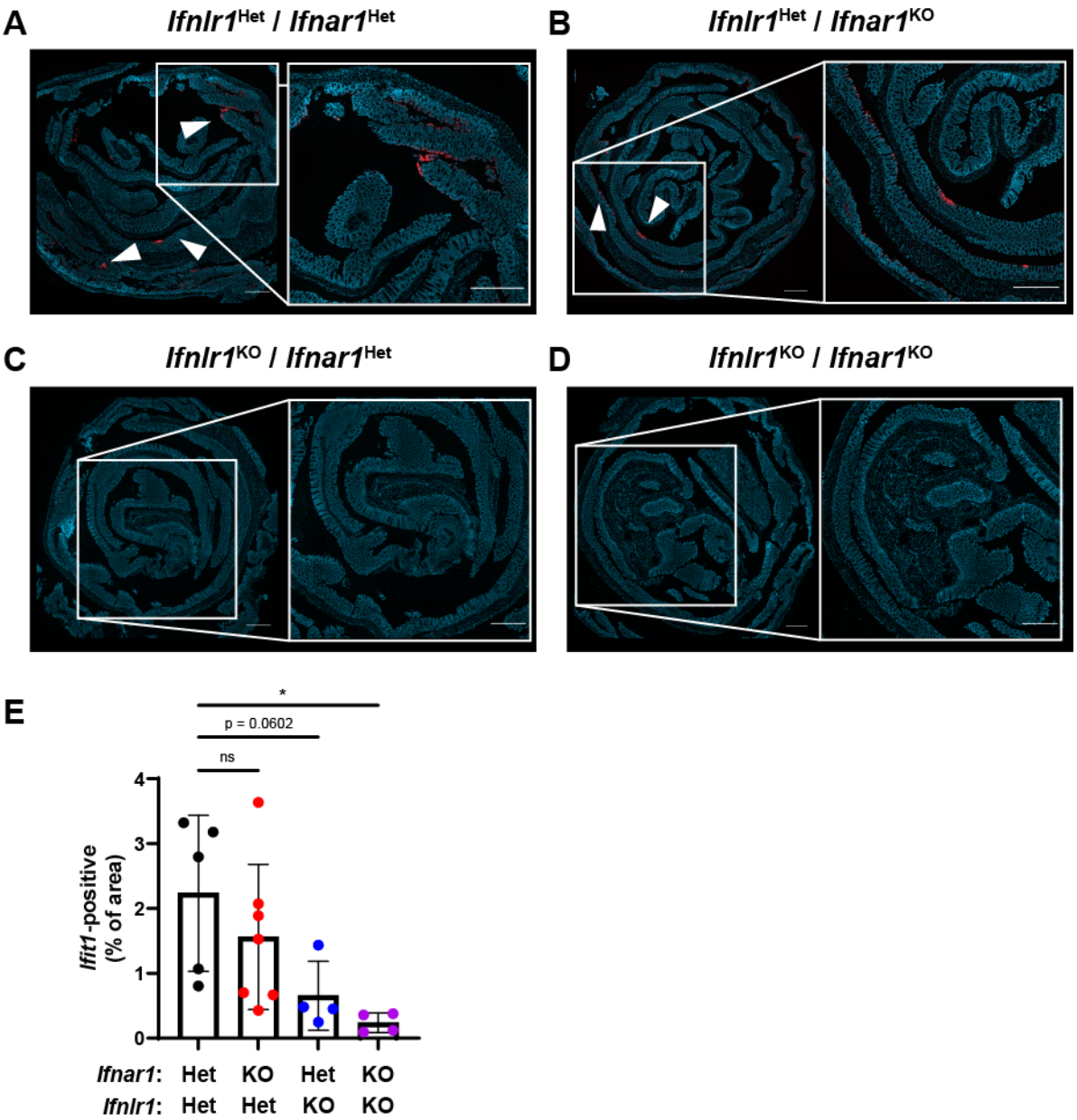

Figure S8. Homeostatic ISG expression is also highly localized in the colon. The colon of *Ifnlr1*^{Het}/*Ifnar1*^{Het}, *Ifnlr1*^{Het}/*Ifnar1*^{KO}, *Ifnlr1*^{KO}/*Ifnar1*^{Het}, and *Ifnlr1*^{KO}/*Ifnar1*^{KO} mice was harvested and stained by RNAscope for the ISG, *Ifit1* (red), with a DAPI (blue) counterstain. Representative images from **(A)** *Ifnlr1*^{Het}/*Ifnar1*^{Het}**,** **(B)** *Ifnlr1*^{Het}/*Ifnar1*^{KO}, **(C)** *Ifnlr1*^{KO}/*Ifnar1*^{Het}, and **(D)** *Ifnlr1*^{KO}/*Ifnar1*^{KO} mice with **(E)** quantification of *Ifit1* area from individual mice. Data are representative of two independent experiments. Scale bar = 500μm.

434 **Mature enterocytes express homeostatic ISGs in public single-cell datasets from mouse**
435 **and human**

436 To determine the extent of conservation of homeostatic ISG expression by IECs, we
437 performed orthogonal analyses of publicly available single-cell RNA-seq (scRNA-seq) datasets
438 from mouse (Haber et al., 2017) and human (Elmentaite et al., 2020) IECs. Recently, Haber et al.
439 published a large single-cell RNA sequencing dataset that profiled sorted IECs from the small
440 intestine of specific-pathogen-free mice and defined 15 distinct IEC subtypes (Haber et al., 2017).
441 We analyzed IECs from this dataset, and found that of the 21 homeostatic ISGs identified in
442 **Figure 1D**, 19 were present in the Haber et al. single-cell dataset. We determined the percentage
443 of each epithelial cell subtype that expresses each individual homeostatic ISG, and generated a
444 heatmap with hierarchical clustering to group IEC subtypes that have similar ISG expression
445 patterns (**Figure 7A**). Homeostatic ISGs were predominantly expressed in mature enterocyte
446 subtypes, which clustered separately from crypt-resident progenitor IECs such as transit
447 amplifying (TA) cells and stem cells (**Figure 7A**). To compare homeostatic ISG expression
448 between polar extremes of the crypt-villus axis, we grouped IEC subtypes that represented
449 enterocytes (mature enterocyte cells) and crypt-associated cells (TA cells and stem cells) to
450 compare the overall proportions of these cells with homeostatic ISG expression. We found that a
451 significantly higher percentage of enterocytes express homeostatic ISGs than crypt-associated
452 cells, but that these homeostatic ISGs were expressed in a relatively small proportion of
453 enterocytes (< 20%) (**Figure 7B**). Notably, *Ifit1* (highlighted in red) was present in ~5% of
454 enterocytes by scRNA-seq, which is consistent with our observation of 1-4% *Ifit1*-positive area by
455 imaging the mouse small intestine (**Figures 6B-G**). Furthermore, the relative absence of ISG-
456 positive crypt-associated cells in this scRNA-seq data is consistent with our observation that
457 intestinal crypts lacked *Ifit1* and *Usp18* expression by imaging.

458 We expanded our investigation to a scRNA-seq dataset from the ileum of healthy, human,
459 pediatric patients that was previously described (Elmentaite et al., 2020). IECs from this dataset

460 were previously clustered by Elmentaite et al and annotated as: enterocytes, early enterocytes,
461 tuft cells, enteroendrocrine cells, BEST4 enterocytes, goblet cells, TA cells, and crypt. For our
462 analysis of homeostatic ISG expression, we excluded IEC sub-types with fewer than 20
463 constituent cells, which retained five annotated groups: enterocytes, early enterocytes, goblet
464 cells, TA cells, and crypt. Of the 21 homeostatic ISGs identified in **Figure 1D**, 14 orthologous
465 human genes were present in these data. Similar to analysis in **Figure 7A,** we determined the
466 percentage of each group that expressed each individual homeostatic ISG and generated a
467 heatmap of these data with hierarchical clustering to group IEC subtypes that have similar ISG
468 expression patterns (**Figure 7C**). Enterocyte, early enterocyte, and goblet subtypes clustered
469 separately from TA cells and crypt, with the highest proportion of homeostatic ISGs being present
470 in the enterocyte subtype (**Figure 7C**). As with mouse IEC data, above, we grouped annotated
471 cells that localize in the crypt (TA cells and crypt) and compared overall proportions of homeostatic
472 ISG expression with the mature enterocyte subtype (**Figure 7D**). Similar to mice, homeostatic
473 ISGs were present in significantly more enterocytes than crypt-associated cells, and most
474 homeostatic ISGs in this human dataset were present in a relatively small proportion of cells (<
475 20%). These human data suggest that ISGs may be present in a small proportion of IECs from
476 healthy, human ileal tissue at homeostasis and may share the localization observed in our murine
477 analyses. Our analysis of a murine scRNA-seq dataset support our previous observations that
478 homeostatic ISGs are not ubiquitously expressed throughout the intestinal epithelium; rather, they
479 are expressed in a minority of IECs and skewed towards mature enterocytes along the crypt-villus
480 axis. Our analysis of a human scRNA-seq dataset are consistent with observations in the murine
481 model, though future studies will be required to definitively address the existence of homeostatic
482 ISGs in human tissue.

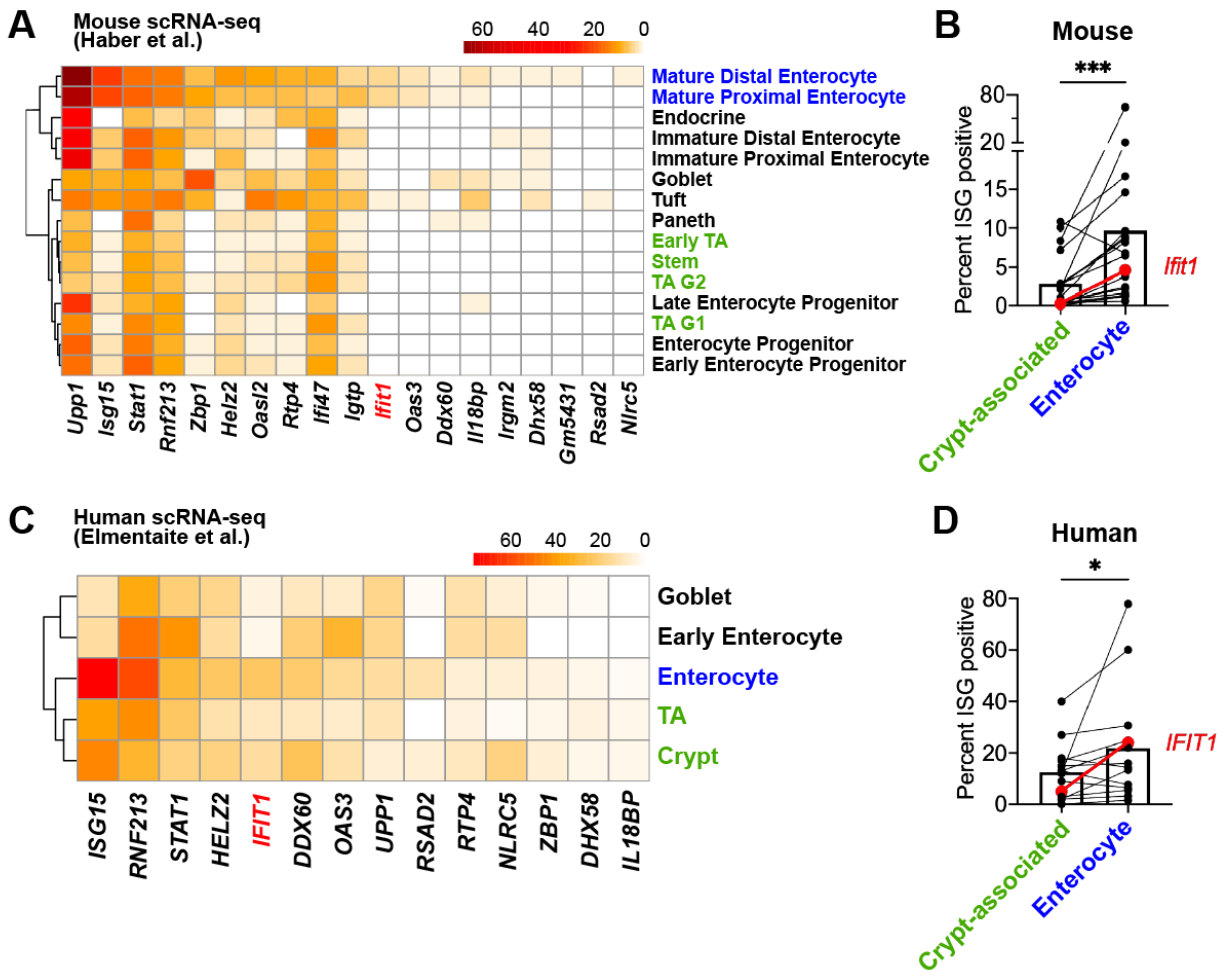

483

484 **Figure 7. Mature enterocytes express homeostatic ISGs in public single-cell datasets from**
485 **mouse and human. A-B.** A mouse IEC single-cell transcriptional dataset (Haber et al., 2017)
486 (GSE92332) was analyzed to determine the percentage of each epithelial cell subtypes that
487 express homeostatic ISGs. **A.** Heatmap depicting the proportion of each epithelial cell type
488 expressing nineteen of the twenty-one homeostatic ISGs identified in **Figure 1**. **B.** Enterocyte
489 subtypes (blue text) and crypt-resident progenitor subtypes (green text) cells were grouped and
490 the percentage of cells that express each homeostatic ISG was compared. **C-D.** A human IEC
491 single-cell transcriptional dataset (Elmentaite et al., 2020) (E-MTAB-8901) was analyzed for the
492 percentage of epithelial cell subtypes that express homeostatic ISGs. **C.** A heatmap depicting the
493 percentage of IEC subtypes that express human orthologs of murine homeostatic ISGs identified

494 in **Figure 1**. **D.** The mature enterocyte subtype (blue text) and crypt-resident progenitor subtypes
495 (green text) were grouped and the percentage of cells that express each homeostatic ISG was
496 compared. Lines in **(B)** and **(D)** link paired ISGs in each IEC subset. Statistical significance in **(B)**
497 and **(D)** was calculated by Wilcoxon test where * = $p < 0.05$, and *** = $p < 0.001$.
498

499 **Assessing the effect of peroral bacterial products on homeostatic ISGs in ABX-treated**
500 **mice**

501 To further define the relationship between bacteria and homeostatic ISGs, we assessed
502 whether oral administration of fecal contents or purified LPS (a bacterial MAMP and TLR4 agonist)
503 could restore localized ISG expression in mice with depleted bacterial microbiota. Control groups
504 of *Ifnlr1*$^{flox/flox}$ mice with conventional microbiota (**Figure 8A**) retained a localized *Ifit1* expression
505 pattern, whereas ABX-treated *Ifnlr1*$^{flox/flox}$ mice (**Figure 8B**) and *Ifnlr1*$^{\Delta IEC}$ mice (**Figure 8C**) lacked
506 *Ifit1* expression. Oral LPS administered to conventional *Ifnlr1*$^{flox/flox}$ mice did not significantly alter
507 the distribution or frequency of localized *Ifit1* expression (**Figure 8D**). However, localized *Ifit1*
508 expression was visible in 4/12 ABX-treated *Ifnlr1*$^{flox/flox}$ mice administered LPS (**Figure 8E, 8H-I**).
509 In ABX-treated *Ifnlr1*$^{flox/flox}$ mice treated with fecal transplant of conventional microbes, localized
510 expression of *Ifit1* was visible in 4/8 mice (**Figure 8F, 8H-I**). Importantly, we did not observe
511 localized *Ifit1* expression in *Ifnlr1*$^{\Delta IEC}$ mice following LPS administration (**Figure 8G**), indicating
512 that LPS-stimulated *Ifit1* depends on IEC expression of *Ifnlr1*.

513 We noted that the visibility of localized *Ifit1* signal following LPS administration or fecal
514 transplant appeared largely binary (i.e. present or absent) in our imaging data (**Figures 8E and**
515 **8F**, representative *Ifit1*-positive and *Ifit1*-negative images). Using quantification of *Ifit1* area
516 (**Figure 8H**), we stratified mice into *Ifit1*-postive and *Ifit1*-negative groups (**Figure 8I-J**) based on
517 a cut-off set at the maximal *Ifit1* area value of *Ifnlr1*$^{\Delta IEC}$ mice (dashed line in **Figure 8H**). Results
518 of this unbiased stratification were consistent with visible *Ifit1* staining and indicated that 8/8
519 conventional *Ifnlr1*$^{flox/flox}$ mice, 0/8 ABX-treated control mice, 4/12 LPS-treated mice, and 4/8 fecal

520 transplant mice were *Ifit1*-positive (**Figure 8I-J**). Statistical analysis by Fisher's exact test
521 indicated that LPS administration non-significantly increased (p = 0.1022) the proportion of mice
522 that were *Ifit1*-positive, whereas fecal reconstitution of ABX-treated mice significantly increased
523 the likelihood of these mice being *Ifit1*-positive (**Figure 8J**). Importantly, mice that received fecal
524 transplant had full restoration of 16S gene copies (**Figure 8K**) despite only 4/8 having homeostatic
525 *Ifit1* expression. These findings suggest that reconstitution of the homeostatic ISG signal by fecal
526 transfer has incomplete penetrance at this timepoint, underscoring the incomplete presence of
527 localized *Ifit1* expression (4/12) in ABX-treated mice administered peroral LPS.

528 To corroborate and extend these findings, we performed orthogonal analyses of *Ifit1*,
529 *Stat1*, and *Oas1a* expression in ileum tissue of WT mice treated with ABX followed by fecal
530 transplant, LPS administration, administration of the TLR5 agonist: flagellin, or administration of
531 TLR9 agonist: CpG DNA (**Figure S9**). Similar to imaging data, these qPCR data exhibited high
532 variance. However**,** stratification of tissues into positive and negative for each ISG indicated that
533 peroral administration of LPS to ABX-treated mice increased the proportion of ISG-positive
534 tissues by 21-36% (*Ifit1*: p=0.065; *Stat1,* p<0.05; *Oas1a*, p<0.05)**.** Additionally, peroral
535 administration of flagellin significantly increased the proportion of ISG-positive mice by 25-44%
536 (*Ifit1*: p=0.052; *Stat1,* p<0.01; *Oas1a*, p<0.05), whereas CpG DNA did not significantly increase
537 the proportion of ISG-positive mice (**Figure S9**). Together, these data suggest that LPS and
538 flagellin are sufficient to stimulate homeostatic ISG expression in a significant proportion of ABX-
539 treated mice. The ability of multiple PRR ligands to stimulate homeostatic ISGs suggests that
540 exposure to a variety of bacterial MAMPs is the basis for localized, homeostatic ISG expression.

541

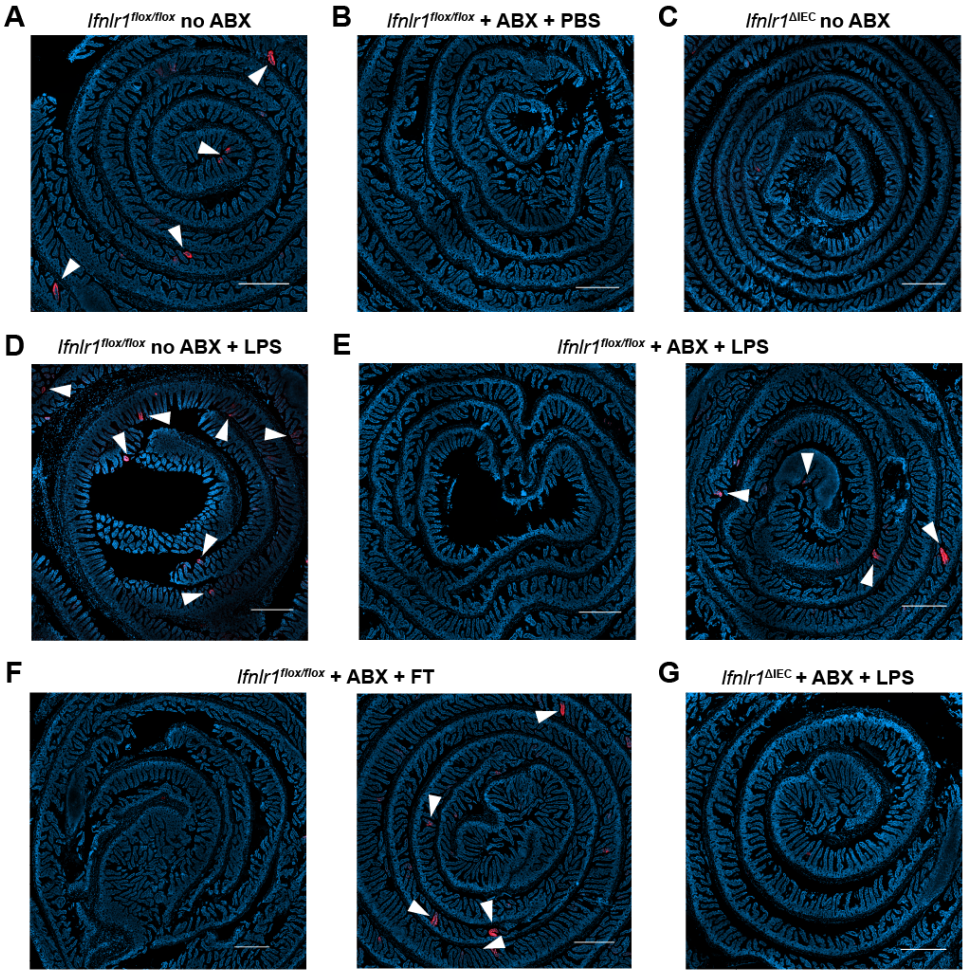

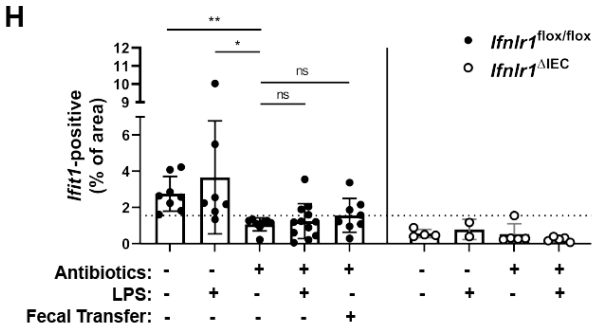

I

ABX	-	-	+	+	+
LPS	-	+	-	+	-
Fecal Transfer	-	-	-	-	+
Ifit1-positive mice / total	8/8	6/7	0/8	4/12	4/8

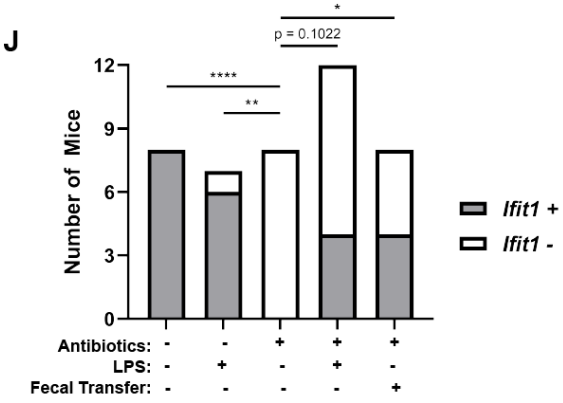

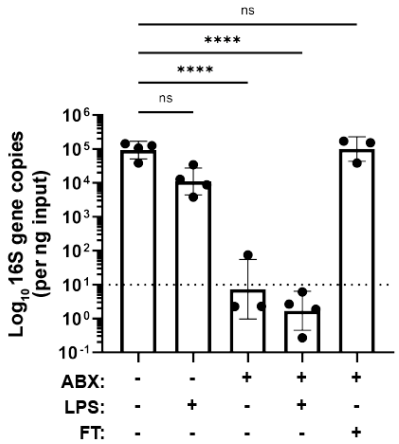

542 **Figure 8. Assessing the effect of peroral bacterial products on localized homeostatic ISGs**
543 **in ABX-treated mice.** The ilea of treated WT, *Ifnlr1*$^{flox/flox}$, and *Ifnlr1*$^{\Delta IEC}$ mice were harvested,
544 processed into Swiss rolls, and stained by *in situ* hybridization for the ISG, *Ifit1* (red), with a DAPI
545 (blue) counterstain**. A-C.** Representative images from *Ifnlr1*$^{flox/flox}$ mice treated with H_2O control
546 followed by PBS stimulation **(A)**, ABX followed by PBS stimulation **(B)**, or from *Ifnlr1*$^{\Delta IEC}$ mice **(B)**.
547 **D.** Representative images of *Ifnlr1*$^{flox/flox}$ mice treated with H_2O control followed by LPS stimulation.
548 **E-F.** Two representative images of *Ifnlr1*$^{flox/flox}$ mice treated with ABX followed by LPS stimulation
549 **(E)** or ABX followed by fecal transplantation **(F)**. **G.** A representative image of *Ifnlr1*$^{\Delta IEC}$ mice
550 treated with ABX followed by LPS stimulation. **H.** Quantification of *Ifit1* area relative to the total
551 area of each tissue section with a dashed line at the highest *Ifnlr1*$^{\Delta IEC}$ value. The proportion of
552 *Ifit1*-positive mice (above dashed line) and *Ifit1*-negative mice (below dashed line) are tabulated
553 **(I)** and graphed **(J)** for *Ifnlr1*$^{flox/flox}$ mice of each condition. **K.** rDNA was isolated from the luminal
554 contents of mice at endpoint harvest. 16S gene copies were assessed by qPCR and normalized
555 to input. Limit of detection: dashed line. Where depicted, scale bar = 500μm. Data points represent
556 individual mice and are pooled from 4 independent experiments in **(A-J)** and from 2 independent
557 experiments in **(K)**. Statistical significance was determined by Kruskal-Wallis with Dunn's multiple
558 comparisons in **(H)**, by one-way ANOVA with Dunnett's multiple comparisons in **(K)**, and by
559 Fisher's exact tests in **(J)** where * = $p < 0.05$, ** = $p < 0.01$, and **** = $p < 0.0001$.

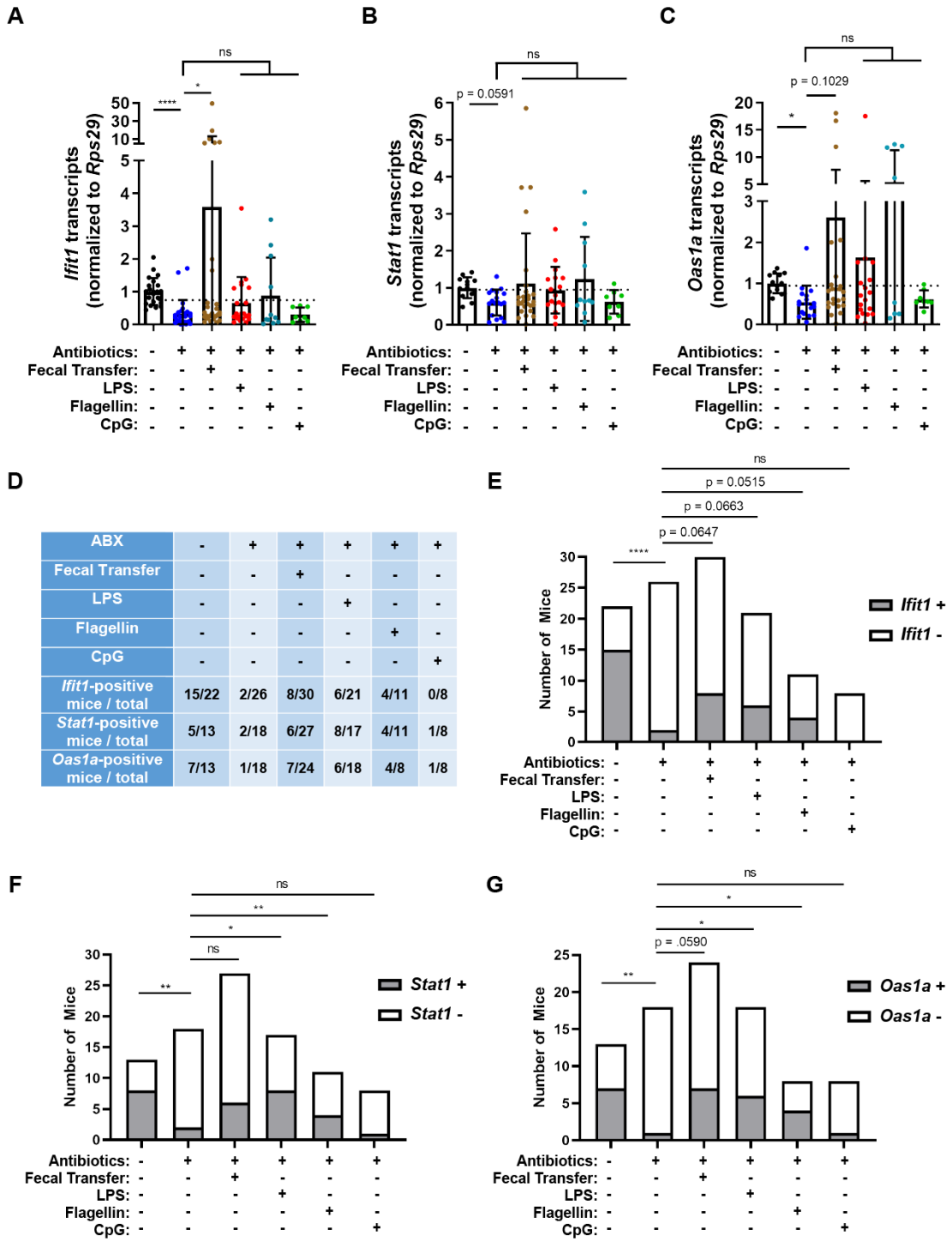

ABX	-	+	+	+	+	+
Fecal Transfer	-	-	+	-	-	-
LPS	-	-	-	+	-	-
Flagellin	-	-	-	-	+	-
CpG	-	-	-	-	-	+
Ifit1-positive mice / total	15/22	2/26	8/30	6/21	4/11	0/8
Stat1-positive mice / total	5/13	2/18	6/27	8/17	4/11	1/8
Oas1a-positive mice / total	7/13	1/18	7/24	6/18	4/8	1/8

Figure S9. Assessing the effect of peroral bacterial products on homeostatic ISGs in ABX-treated mice. The ileum of treated WT, *Ifnlr1*$^{flox/flox}$, and *Ifnlr1*$^{\Delta IEC}$ mice was harvested and *Ifit1* **(A)**, *Stat1* **(B)**, and *Oas1a* **(C)** was quantified by qPCR. Delineation of positive ISG expression was

564 conservatively selected as one standard deviation above the mean of ABX-treated mice (dashed
565 line). Mice were binned into ISG-positive (above dashed line) or ISG-negative (below dashed line)
566 groups and are tabulated for each condition in **D**. The proportion of mice with expression of *Ifit1*
567 **(E)**, *Stat1* **(F)**, and *Oas1a* **(G)** are graphed for each condition. Data points represent individual
568 mice and are pooled from 3-9 independent experiments. Statistical significance was determine
569 by Kruskal-Wallis with Dunn's multiple comparisons **(A-C)** and by Fisher's exact test **(E-G)** where
570 * = $p < 0.05$, ** = $p < 0.01$, and **** = $p < 0.0001$.
571

572 **The homeostatic IFN-λ response preemptively protects IECs from murine rotavirus**
573 **infection**

574 To assess the capacity of homeostatic ISGs to protect IECs from viral infection, we utilized
575 infection with murine rotavirus (mRV), an IEC-tropic pathogen. Prior studies of rotaviruses have
576 identified viral immune evasion genes that block IFN induction through multiple mechanisms
577 (Arnold et al., 2013). However, we reasoned that pre-existing ISG expression stimulated by the
578 bacterial microbiome at homeostasis may preemptively protect IECs from the infection before
579 viral gene expression is initiated. To determine the role of an epithelial IFN-λ response over the
580 course of mRV infection in adult mice, we monitored daily shedding of viral genomes in the stool
581 of *Ifnlr1*$^{flox/flox}$ mice and *Ifnlr1*$^{\Delta IEC}$ littermates. We first detected mRV shedding in the stool on day
582 two after inoculation and, at this early timepoint, *Ifnlr1*$^{\Delta IEC}$ mice shed 20-fold more mRV genomes
583 into their stool than *Ifnlr1*$^{flox/flox}$ mice (**Figure 9A**). However, at the peak of viral shedding between
584 days three and five, there were no significant differences between *Ifnlr1*$^{flox/flox}$ and *Ifnlr1*$^{\Delta IEC}$
585 littermates (**Figure 9A**). This similarity at peak of viral shedding was consistent with an ability of
586 mRV to evade the host IFN response once infection is established. Together, these findings
587 suggest that *Ifnlr1*$^{\Delta IEC}$ mice have defects in protection against initiation of mRV infection and that
588 the protective capacity of endogenous IFN-λ signaling against mRV is primarily prophylactic in
589 nature.

590 To more stringently assess the capacity of *Ifnlr1* to protect IECs against the earliest stages
591 of mRV infection, we inoculated mice with 5000 SD50 (50% shedding dose) of mRV to maximize
592 the likelihood of uniform viral exposure throughout the intestine. At 24 hours post-inoculation, we
593 quantified mRV genomes in the epithelial fraction and the proportion of infected IECs (live,
594 EpCAM-positive, CD45-negative, and mRV-positive) by flow cytometry. At 24 hours post-
595 inoculation, we found that *Ifnlr1*$^{\Delta IEC}$ mice had 20-fold more mRV genomes than *Ifnlr1*$^{flox/flox}$ mice
596 (**Figure 9B**). In addition, we found that a three-fold greater proportion of IECs were infected with
597 mRV in *Ifnlr1*$^{\Delta IEC}$ mice than *Ifnlr1*$^{flox/flox}$ mice at 24 hours post-infection (**Figures 9C-F**). However,
598 the median fluorescence intensity (MFI) of mRV antigen was equivalent in mRV-infected IECs
599 from *Ifnlr1*$^{flox/flox}$ and *Ifnlr1*$^{\Delta IEC}$ mice (**Figure 9G**) and the MFI of mRV did not correlate ($r^2 = 0.0003$)
600 with the percentage of infected IECs (**Figure 9H**). This equivalent mRV antigen burden in infected
601 cells from *Ifnlr1*$^{flox/flox}$ and *Ifnlr1*$^{\Delta IEC}$ mice in combination with the lack of correlation between antigen
602 burden and percentage of infected cells suggests that the protective role of *Ifnlr1* is to prevent
603 infection of IECs rather than to limit replication within IECs after they are infected. We assessed
604 an earlier timepoint at 12 hours post-inoculation and observed similar trends toward an increased
605 proportion of IEC infection in *Ifnlr1*$^{\Delta IEC}$ relative to *Ifnlr1*$^{flox/flox}$ littermates, but the extent of infection
606 was 10-100 fold lower and near the limit of detection (**Figure S10**). Thus, the 12- and 24-hour
607 timepoints capture the earliest detectable infection of IECs by mRV, and this early infection is
608 significantly reduced by IFN-λ signaling.

609 To further contextualize the localization of ISGs and mRV-infected cells over time, we
610 performed *in situ* hybridization for mRV genomes and *Ifit1* in the ileum of WT mice at 12, 24, and
611 96 hours post-inoculation. Quantification of co-staining for *Ifit1* in mRV-infected cells indicated
612 that a minority (~30%) were *Ifit1*+ at 12hr or 24hr post-inoculation, whereas a majority (~63%) of
613 mRV-infected cells were *Ifit1*+ at 96hr post-inoculation (**Figure 9I-J, S11**). These co-staining data
614 are consistent with early mRV evasion of IFN responses within infected IECs, at the same
615 timepoints that we observed increased infection of *Ifnlr1*$^{\Delta IEC}$ mice (**Figures 9B-F, S10**).

616 Furthermore, we found mRV inoculation did not increase the area of *Ifit1* expression in the
617 intestine at 12-24 hours post-inoculation. However, at 96 hours post-inoculation, we found a
618 significant increase in epithelial *Ifit1* expression in the ileum that coincided with increased viral
619 genomes and antigen (**Figure S12**), suggesting that *Ifit1* expression at 12 and 24 hours post-
620 inoculation is primarily due to the preexisting homeostatic response rather than in response to
621 mRV infection. Therefore, we propose that homeostatic ISGs stimulated by *Ifnlr1* expression on
622 IECs plays an early protective role against viral infection that preempts viral IFN evasion
623 mechanisms.

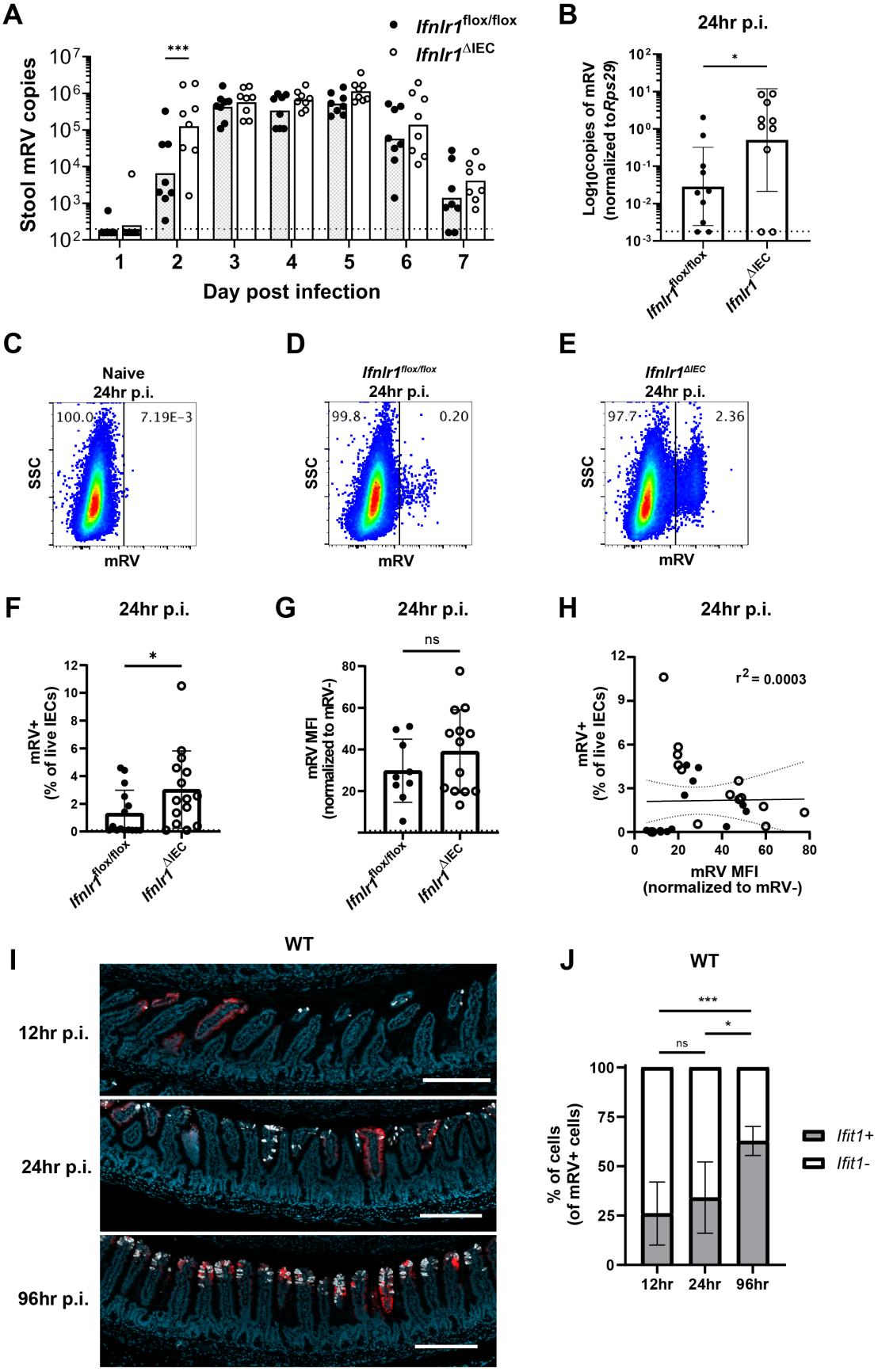
A
Ifnlr1flox/flox
Ifnlr1ΔIEC
Stool mRV copies
Day post infection
***
B
24hr p.i.
Log10copies of mRV (normalized toRps29)
*
C
Naive
24hr p.i.
100.0
7.19E-3
SSC
mRV
D
Ifnlr1flox/flox
24hr p.i.
99.8
0.20
E
Ifnlr1ΔIEC
24hr p.i.
97.7
2.36
F
24hr p.i.
mRV+ (% of live IECs)
G
ns
mRV MFI (normalized to mRV-)
H
r2 = 0.0003
mRV MFI (normalized to mRV-)
I
WT
12hr p.i.
24hr p.i.
96hr p.i.
J
WT
% of cells (of mRV+ cells)
Ifit1+
Ifit1-
12hr
24hr
96hr

624

625 **Figure 9. The homeostatic IFN-λ response preemptively protects IECs from murine**
626 **rotavirus infection.** *Ifnlr1*$^{flox/flox}$ and *Ifnlr1*$^{\Delta IEC}$ mice were infected with 100 SD50 **(A)** or 5000 SD50
627 **(B-H)** of mRV and stool **(A)** or stripped ileal intestinal epithelial cells **(B-G)** were assessed for
628 mRV infection. **A.** Timecourse of mRV genome copies detected in the stool of *Ifnlr1*$^{flox/flox}$ and
629 *Ifnlr1*$^{\Delta IEC}$ mice by qPCR. **B-G.** Mechanically stripped intestinal epithelial cell fractions were
630 analyzed by qPCR for mRV genome copies **(B)** or flow cytometry for mRV antigen-positive IECs
631 **(C-G).** Representative flow cytometry plots of naïve **(C)**, *Ifnlr1*$^{flox/flox}$ **(D)**, and *Ifnlr1*$^{\Delta IEC}$ **(E)** mice
632 infected with mRV with quantification in **(F)**. **G.** The MFI of mRV antigen in infected cells relative
633 to uninfected cells. **H.** A linear correlation plot of mRV+ cells and mRV MFI with 95% confidence
634 intervals (dashed lines). **I-J.** WT mice were infected with 5000 SD50 of mRV and the ilea were
635 processed into Swiss rolls and stained by *in situ* hybridization for the ISG, Ifit1, or murine rotavirus.
636 The percentage of mRV-infected cells that were *Ifit1*-positive and *Ifit1*-negative were determined.
637 Additional representative images for **(I-J)** are depicted in **Figure S11**. Where designated in **(A-**
638 **G)**, dashed lines = LOD as set by naïve mice. Data points represent individual mice and are
639 pooled from 2-3 independent experiments. Statistical significance was determined by two-way
640 ANOVA with Sidak's multiple comparisons **(A)**, by Mann Whitney **(B, F)**, unpaired t-test **(G)**, or
641 Kruskal-Wallis with Dunn's multiple comparisons **(J)**, where * = $p < 0.05$ and *** = $p < 0.001$.

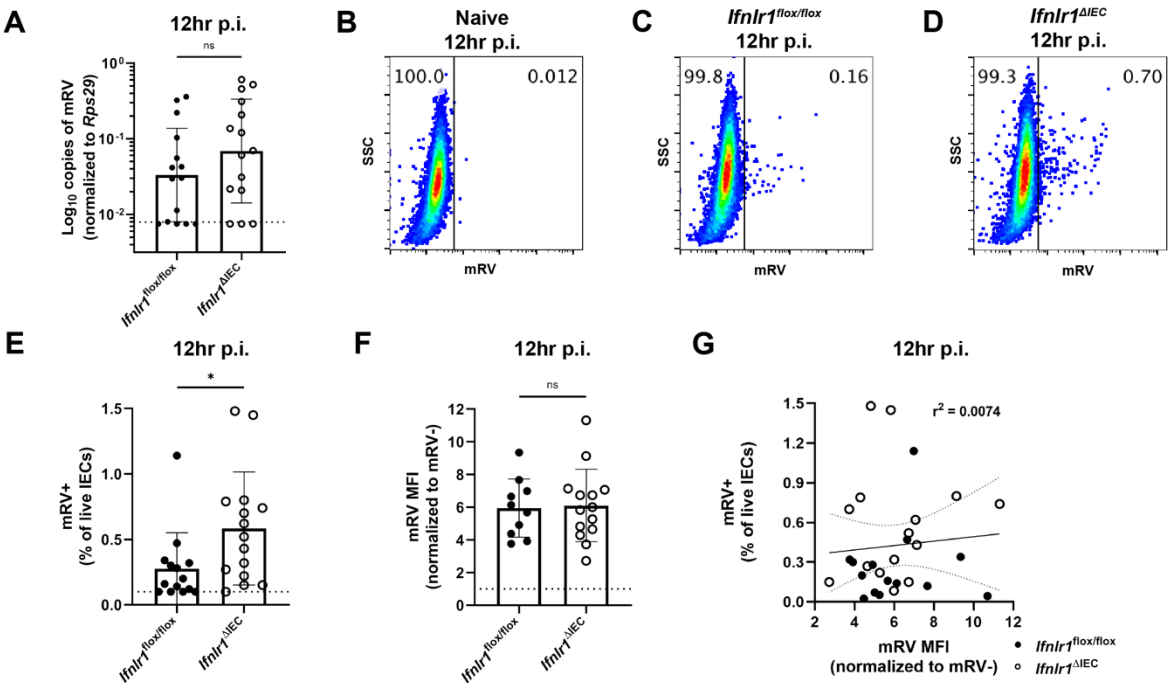

642

643 **Figure S10. The homeostatic IFN-λ response preemptively protects IECs from murine**
644 **rotavirus infection.** *Ifnlr1*$^{flox/flox}$ and *Ifnlr1*$^{\Delta IEC}$ mice were infected with 5000 SD50 of mRV by oral
645 gavage and stripped ileal intestinal epithelial cell fractions were analyzed by qPCR for mRV
646 genome copies **(A)** or flow cytometry for mRV antigen-positive IECs **(B-F)**. Representative flow
647 cytometry plots of naïve **(B)**, *Ifnlr1*$^{flox/flox}$ **(C)**, and *Ifnlr1*$^{\Delta IEC}$ **(D)** mice infected with mRV. **E.** The
648 percentage of mRV+ live IECs for each genotype. **F.** The MFI of mRV antigen in infected cells
649 relative to uninfected cells. **G.** A linear correlation plot of mRV+ cells and mRV MFI with 95%
650 confidence intervals (dashed lines). Where designated in **(A, E-F)**, dashed lines = LOD as set by
651 naïve mice. Data points represent individual mice and are pooled from 3 independent
652 experiments. Statistical significance was calculated by Mann Whitney **(A, E)**, or unpaired t-test
653 **(F)** where * = $p < 0.05$.

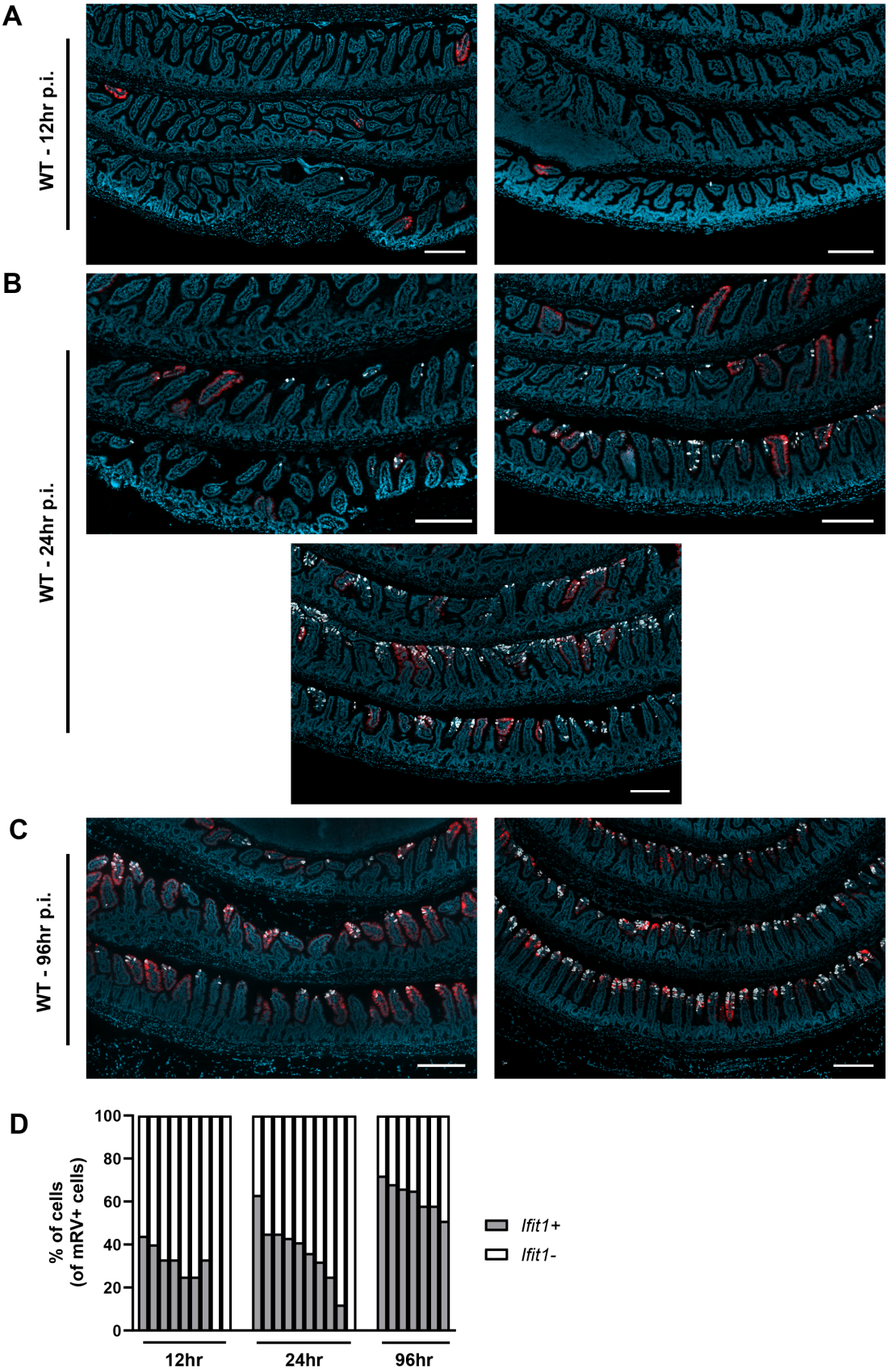
A
WT - 12hr p.i.
B
WT - 24hr p.i.
C
WT - 96hr p.i.
D
% of cells
(of mRV+ cells)
100
80
60
40
20
0
12hr
24hr
96hr
Ifit1+
Ifit1-

654

Figure S11. mRV and *Ifit1* co-incidence. WT mice were infected with 5000 SD50 of mRV by oral gavage and the ilea were processed into Swiss rolls and stained by *in situ* hybridization for the ISG, *Ifit1* (red), and mRV RNA (white), with a DAPI (blue) counterstain. Representative images of ileum from **(A)** 12hr post-inoculation, **(B)** 24hr post-inoculation, and **(C)** 96hr post-inoculation, where each image represents an individual mouse. **D**. The percentage of mRV-infected cells that are *Ifit1*-positive and negative for each individual mouse. Where displayed, scale bar = 200μm.

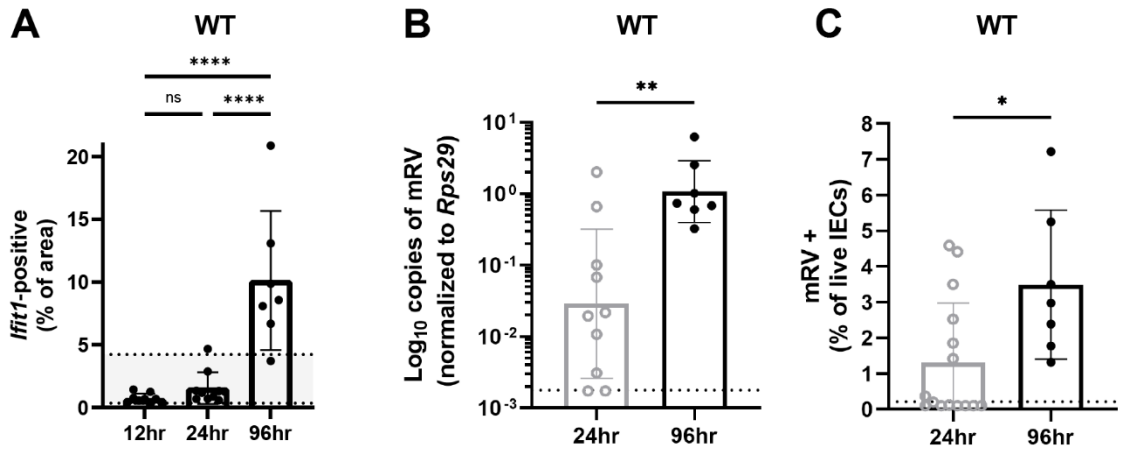

Figure S12. Murine rotavirus infection increases the distribution of *Ifit1* expression at late times post-inoculation. WT mice were infected with 5000 SD50 of mRV and the ilea were processed into Swiss rolls and stained by *in situ* hybridization for the ISG, *Ifit1* (red) with a DAPI (blue) counterstain. **A.** Quantification of *Ifit1* area relative to the total area of each tissue section with highlighted area representing historical range of *Ifit1* area in naive WT mice. In parallel, stripped ileal intestinal epithelial cell fractions were analyzed by qPCR for mRV genome copies **(B)** or flow cytometry for mRV antigen-positive IECs **(C)**. For comparison in **(B-C)**, 24hr data is historical and duplicated from *Ifnlr1*$^{flox/flox}$ samples presented in **Figure 9**. Where displayed, scale bar = 500μm, and where designated, dashed lines = LOD as set by naïve mice. Data points represent individual mice and are pooled from 2 independent experiments. Statistical significance was calculated by one-way ANOVA with Tukey's multiple comparisons **(A)** and Mann Whitney **(B-C)**, where ** = $p < 0.005$ and **** = $p < 0.0001$.

674 **Discussion**

675 Here, we report that bacterial microbiota induce an enteric IFN-λ response in IECs at
676 homeostasis (**Figures 1-4**). Although there are previous reports of basal, non-receptor-dependent
677 ISG expression in immortalized and primary cell lines (Hakim et al., 2018), the homeostatic
678 response that we report here is dependent on the IFN-λ receptor. Furthermore, we find this
679 response is independent of type I IFN signaling (**Figure 3**), indicating that IFN-λ signaling plays a
680 dominant and active role in the gastrointestinal epithelium. We also find minimal changes in ISG
681 expression within the spleen and MLN after ABX treatment, suggesting that homeostatic ISGs
682 are predominantly expressed in the intestine. These findings differ slightly from prior descriptions
683 of systemic type I IFN responses that are dependent on bacterial microbiota (Abt et al., 2012;
684 Bradley et al., 2019; Ganal et al., 2012; Steed et al., 2017; Stefan et al., 2020; Winkler et al.,
685 2020). However, differences in the specific tissues and cell types analyzed make it difficult to draw
686 direct comparisons across these studies. Therefore, we conclude that homeostatic ISGs are
687 substantially present in IECs, but do not dispute the prior findings that relatively low homeostatic
688 ISG expression induced by type I IFN plays an important role in extra-intestinal tissues and non-
689 epithelial cell types.

690 A prior study by Mahlakõiv et al. noted the presence of *Ifnl2/3* transcripts in CD45+ cells
691 within the stripped intestinal epithelium, but not the lamina propria, at homeostasis. We have
692 confirmed these findings and have extended them to show that this homeostatic expression of
693 *Ifnl2/3*, but not *Ifnb1*, is dependent on bacterial microbiota (**Figure 5**). However, we have been
694 unable to detect IFN-λ transcripts by RNA scope *in situ* hybridization in mice at homeostasis,
695 consistent with recently published data (Ingle et al., 2021). This suggests that the production of
696 IFN-λ is below the limit of detection by imaging or highly transient in nature. It is also unclear
697 which CD45+ cell type produces homeostatic IFN-λ. Swamy et al. showed that T cell receptor
698 stimulation led intraepithelial lymphocytes to produce IFN-λ (Swamy et al., 2015) and Mahlakõiv
699 et al. suggested that the primary producers of IFN-λ at steady-state are intraepithelial lymphocytes

700 due to the abundance of intraepithelial lymphocytes in the epithelial fraction. However, myeloid
701 cells also reside near the intestinal epithelium and can sample luminal contents by various
702 mechanisms (Chieppa et al., 2006; McDole et al., 2012; Niess et al., 2005). Although the cell type
703 that produces homeostatic IFN-λ is unknown, enrichment for *Ifnl2/3* in CD45+ cells within the
704 intestinal epithelial fraction suggests that proximity to bacterial stimuli may be a primary
705 determinant in this response. We suggest that these cells may be actively surveying the intestinal
706 epithelium to detect bacterial MAMPs. The specific CD45+ cell types responsible for producing
707 homeostatic IFN-λ will be a topic of interest for future studies.

708 We initially anticipated that the distribution of homeostatic ISGs would be uniform among
709 IECs. Instead, we found that this IFN-λ response is highly localized within enteric tissues.
710 Homeostatic ISGs are observed in a minority of small intestinal villi and are primarily present in
711 mature epithelium towards the villus tips (**Figure 6**). Likewise, homeostatic ISGs are present
712 within patches of the mature epithelium in the colon (**Figure S8**). The surprising finding of
713 localized ISGs in the ileum are supported by analysis of independently-generated scRNA-seq
714 datasets from mouse and human small intestinal IECs that depict expression of homeostatic ISGs
715 in a minority of cells with predominant expression in mature enterocytes (**Figure 7**).

716 The basis for localized ISG expression is unknown; however, it may reflect the distribution
717 of cells capable of sensing bacterial microbiota, distinct microenvironments within the
718 gastrointestinal tract, or qualitative differences in bacterial colonization. Given the results of our
719 data in **Figures 8** and **Figure S9**, we suggest that LPS administration, flagellin administration, or
720 fecal transplant can partially restore the expression of homeostatic ISGs in the small intestine.
721 This interpretation supports the concept that localized ISG-positive regions may be uniquely
722 exposed or responsive to a variety of bacterial MAMPs. Indeed, we find that MYD88 is required
723 for WT levels of homeostatic ISG expression in the small intestine (**Figure 3**). However, MYD88
724 is dispensable for homeostatic ISG expression in the colon, and TRIF is not required in either
725 small intestine or colon (**Figure 3**). These data suggest that the bacterial microbiota broadly

726 stimulates homeostatic IFN-λ through multiple, redundant PRRs. Furthermore, the presence of
727 localized *Ifit1* expression in ABX-treated mice following LPS administration (**Figure 8**) suggests
728 that localization is an intrinsic property of homeostatic ISG stimulation and is not likely to be due
729 to qualitative differences in bacterial colonization.

730 ISG localization may be indicative of regional differences in access of luminal bacterial
731 MAMPs to IFN-λ-producing cells. One host mechanism to limit bacterial interactions with the
732 intestinal epithelium is the presence of mucus layers (Atuma et al., 2001; Johansson et al., 2011).
733 Intriguingly, the single mucus layer in the small intestine is much less adherent than the mucus
734 layers present in the colon (Johansson et al., 2011), which might allow occasional direct bacterial
735 interactions with IECs or other cells near the intestinal epithelium. However, soluble components
736 from enteric bacteria may also readily diffuse through mucus layers. In this case, there may be
737 sporadic defects in tight junction proteins that are required to maintain the intestinal epithelium.
738 Tight junction remodeling is essential to maintain intestinal integrity during apoptosis and
739 extrusion of IECs that are regularly shed from the intestinal epithelium (Williams et al., 2015).
740 Future studies will be necessary to determine whether defects in epithelial barrier integrity during
741 extrusion events are linked to the local ISG responses that we observe and further delineation of
742 the factors that render specific regions "responsive" will be of great interest for follow-up studies.

743 The preceding findings (**Figure 4)** suggested that the homeostatic ISG response in IECs
744 would provide protection against IEC-tropic viruses, such as mRV. Although bacterial-associated,
745 IFN-independent mechanisms of mRV clearance have been reported (Shi et al., 2019; Zhang et
746 al., 2014), we found that the signature of homeostatic ISGs in ileum tissue included well-
747 characterized antiviral ISGs (**Figures 1-2**). To investigate whether these homeostatic ISGs
748 protect against MRV, we used *Ifnlr1*$^{\Delta IEC}$ mice that lack homeostatic ISGs (**Figure 4 and 6**) rather
749 than using ABX-treatment, which introduces pleiotropic effects on rotavirus infection (Uchiyama
750 et al., 2014) and dramatically increases transit time through the intestine (Baldridge et al., 2015).
751 Using *Ifnlr1*$^{\Delta IEC}$ mice, we found increase in IEC infection by mRV at early stages of infection

752 compared to *Ifnlr1*$^{flox/flox}$ littermates (**Figure 9** and **Figure S10**). However, the protection offered
753 by IEC expression of *Ifnlr1* was lost by the middle and late stages of infection, consistent with the
754 ability of mRV to antagonize induction of IFN responses once infection is established (Arnold et
755 al., 2013). Our observations during initiation of infection may provide important context to
756 observations in other studies that report differing capacity for infection-induced IFN-λ to protect
757 against mRV infection (Lin et al., 2016; Pott et al., 2011). Ultimately, it is clear that prophylactic
758 administration of exogenous IFN-λ protects against mRV infection (Lin et al., 2016; Pott et al.,
759 2011; Van Winkle et al., 2020), providing precedent that homeostatic IFN-λ would also be
760 protective when induced by bacterial microbiota prior to infection.

761 Although we found that homeostatic ISGs provide protection during initiation of mRV
762 infection, it remains unclear how these localized ISG pockets impart this protection. Given our
763 findings in **Figure 8** and **Figure S9**, we suggest that these localized ISGs may be indicative of
764 locations that are particularly vulnerable to viral infection if ISGs were not present at the time of
765 viral exposure. However, alternative explanations for the protective effects that we observe are
766 also plausible, such as: i) an inability to detect the full magnitude of ISG expression by imaging,
767 or ii) an unknown temporal component to homeostatic ISG signaling that may be coincident with
768 durable ISG protein expression. Given the magnitude of signal amplification in RNAscope *in situ*
769 hybridization and the similarity of *Ifit1* expression in our imaging data to *Ifit1* expression in public
770 single-cell sequencing datasets, we find it unlikely that there is more widespread homeostatic ISG
771 expression below the limit of our detection by imaging. However, we do think an uncharacterized
772 temporal component of homeostatic ISG signaling is plausible, wherein individual villi may be
773 rapidly and transiently expressing homeostatic ISGs in response to sensing of bacterial
774 microbiota. This temporal model may also include a more durable ISG protein response that is
775 not fully concordant with expression of ISG transcripts. In sum, these findings indicate that
776 preexisting, homeostatic ISGs present in *Ifnlr1*-sufficient mice are protective during initiation of
777 mRV infection, but that endogenous IFN-λ does not reduce mRV burden in infected cells. These

778 data highlight the possibility that detection of bacterial microbiota in particularly exposed areas
779 may preemptively activate homeostatic ISGs as a form of anticipatory immunity to protect the
780 intestinal epithelium from enteric viruses.

781 **Methods**

782 **Mice**

783 All mice were bred using the C57BL/6 background and used within the age of 8-12 weeks;
784 C57BL/6J mice (stock # 000664) were purchased from Jackson Laboratories (Bar Harbor, ME)
785 and used as wild-type. Genetically modified mice included *Ifnlr1*$^{-/-}$ and *Ifnlr1*$^{flox/flox}$ (generated from
786 *Ifnlr1*$^{tm1a(EUCOMM)Wtsi}$ as published (Baldridge et al., 2017)), *Ifnar1*$^{-/-}$ (B6.129.Ifnar1^{tm1}), *Trif*$^{-/-}$ (JAX
787 C57BL/6J-*Ticam1*^{Lps2}/J, stock #005037), *Myd88*$^{-/-}$ (JAX B6.129P2(SJL)-*Myd88*$^{tm1.1Defr}$/J, stock
788 #009088), *Irf3*$^{-/-}$ (B6.129S/SvEv-Bcl2l12/Irf3^{tm1Ttg}), *Irf7*$^{-/}$ (B6.129P2-Irf7tm1Ttg/TtgRbrc), *Stat1*$^{-/-}$
789 (B6.129.-*Stat1*^{tm1Dlv}), and Villin-cre (B6.Cg-Tg(Vil1-cre)997Gum/J) mice. *Ifnlr1*$^{-/-}$ and *Ifnar1*$^{-/-}$ mice
790 were bred to *Ifnlr1*^{Het}/*Ifnar1*^{Het} mice to generate littermate *Ifnlr1*^{Het}/*Ifnar1*^{Het}, *Ifnlr1*^{Het}/*Ifnar1*^{KO},
791 *Ifnlr1*^{KO}/*Ifnar1*^{Het}, *Ifnlr1*^{KO}/*Ifnar1*^{KO} offspring.

792 All mice were maintained in specific-pathogen-free facilities at Oregon Health & Science
793 University (OHSU) and Washington University in St. Louis (WUSTL). Animal protocols were
794 approved by the Institutional Animal Care and Use Committee at OHSU (protocol #IP00000228)
795 and WUSTL (protocol #20190162) in accordance with standards provided in the *Animal Welfare*
796 *Act*.

797 For all experiments, mice were allocated into experimental groups based on genotype with
798 equal representation of individual litters and equal sex ratios.

799 **Mouse Treatments**

800 Mice were administered an *ad libitum* antibiotic cocktail consisting of: 1 g/L ampicillin, 1
801 g/L metronidazole, 1 g/L neomycin, and 0.5 g/L vancomycin (Sigma, St. Louis, MO) in autoclaved
802 H_2O (OHSU) or in 20 mg/mL grape Kool-Aid (Kraft Foods, Northfield, IL) (WUSTL). Sterile H_2O
803 (OHSU) or Kool-Aid (WUSTL) alone was used as a control. Mice were maintained on antibiotics
804 or control for 2 weeks prior to harvest.

805 Recombinant IFN-λ was provided by Bristol-Myers Squibb (New York City, NY) as a
806 monomeric conjugate comprised of 20kDa linear PEG attached to the amino-terminus of murine

807 IFN-λ. Mice were injected intraperitoneally with IFN-λ or an equal volume of PBS vehicle as
808 indicated in figure legends at the indicated time prior to analysis.

809 Mice were stimulated with of 100µg of the synthetic dsRNA analogue, poly I:C (R&D,
810 #4287) or PBS by intraperitoneal injection in a 200µL volume, 2 hours prior to harvest.

811 25µg of the bacterial product lipopolysaccharide (Sigma #L4391), flagellin (Invivogen #tlrl-
812 bsfla; from *Bacillus subtilis*) or CpG (Invivogen #tlrl-1585; Class A CpG oligonucleotide) were
813 perorally administered to mice in 25µL of sterile PBS. Mice were treated on days 15 and 16 of
814 antibiotic treatment or H_2O control prior to harvest on day 17.

815 For transplantation of fecal material, antibiotic treatment was stopped and mice were fed
816 25uL of fecal mixture by pipet for two consecutive days. Fecal mixture was prepared by collecting
817 fecal samples from control mice; a single stool pellet was resuspended in 200uL of sterile PBS,
818 stool was broken apart by pipetting, and large particulate was allowed to settle for several minutes
819 prior to administration.

820 **Cell Isolation**

821 Epithelial fractions were prepared by non-enzymatic dissociation as previously described
822 (Nice et al., 2016). Briefly, mouse ileum was opened longitudinally and agitated by shaking in
823 stripping buffer (10% bovine calf serum, 15 mM HEPES, 5 mM EDTA, and 5 mM dithiothreitol
824 [DTT] in PBS) for 20 min at 37°C. Lamina propria fractions were prepared by enzymatic digestion
825 and dissociation with the Lamina Propria Dissociation Kit and GentleMacs Dissociator (Miltenyi
826 Biotec, Bergisch Gladbach, Germany). Dissociated cells were collected for use in qPCR analysis,
827 flow cytometry, and magnet enrichment.

828 **Rotavirus infection of mice**

829 Mouse rotavirus (EC strain) was graciously provided by Andrew Gewirtz (Georgia State
830 University). Viral stocks were generated by inoculating 4- to 6-day-old neonatal BALB/c mice and
831 harvesting the entire gastrointestinal tract upon presentation of diarrheal symptoms 4 to 7 days
832 later. Intestines were freeze-and-thawed, suspended in PBS, and homogenized in a bead beater

833 using 1.0-mm zirconia-silica beads (BioSpec Products). These homogenates were clarified of
834 debris, aliquoted, and stored at -70°C. The 50% shedding dose (SD50) was determined by
835 inoculation of 10-fold serial dilutions in adult C57BL/6J mice. For stool time-course studies, mice
836 were inoculated by peroral route with 100 SD50 and a single stool pellet was collected daily for
837 viral quantitation by qPCR. For protection studies, mice were inoculated by intragastric gavage
838 with 5000 SD50, and ileum was isolated and mechanically stripped 12- and 24-hours later for
839 quantitation of viral burden by qPCR and flow cytometry.

840 **RNA isolation, rDNA isolation, qPCR, and analysis**

841 RNA from tissue and stripped IECs was isolated with TRIzol (Life Technologies, Carlsbad,
842 CA) according to the manufacturer's protocol. RNA from magnet-enriched cells was purified by
843 Zymo *Quick*-RNA Viral Kit (Zymo Research, Irvine, CA). The larger of either 1µg of RNA or 5µL
844 of RNA were used as a template for cDNA synthesis by the ImProm-II reverse transcriptase
845 system (Promega, Madison, WI) after DNA contamination was removed with the DNAfree kit (Life
846 Technologies). 16S bacterial rDNA was isolated from stool and intestinal contents with a
847 ZymoBIOMICS DNA kit (Zymo Research, Irvine, CA) kit. Quantitative PCR was performed using
848 PerfeCTa qPCR FastMix II (QuantaBio, Beverly, MA) and the absolute quantities of transcript
849 were determined using standard curves composed of gBlocks (IDT) containing target sequences.
850 Absolute copy numbers from tissue samples were normalized to the housekeeping gene,
851 ribosomal protein S29 (*Rps29*). Taqman assays for selected genes were ordered from IDT
852 (Coralville, IA): *Rps29* (Mm.PT.58.21577577), *Ifit1* (Mm.PT.58.32674307), *Oas1a*
853 (Mm.PT.58.30459792), *Mx2* (Mm.PT.58.11386814), *Stat1* (Mm.PT.58.23792152), *Isg15*
854 (Mm.PT.58.41476392.g). Taqman assays for *Ifnl2/3* and *Ifnb1* were designed previously (Van
855 Winkle et al., 2020) and consisted of the following primer-probe sequences: *Ifnl2/3* (Primer 1 –
856 GTTCTCCCAGACCTTCAGG, Primer 2 – CCTGGGACCTGAAGCAG, Probe –
857 CCTTGCAGGCTGAGGTGGC); *Ifnb1* (Primer 1 – CTCCAGCTCCAAGAAAGGAC, Primer 2 –
858 GCCCTGTAGGTGAGGTTGAT, Probe – CAGGAGCTCCTGGAGCAGCTGA). Murine rotavirus

859 was detected using Taqman primer-probe sets specific for 422-521 of GeneBank sequence
860 DQ391187 as previously described (Fenaux et al., 2006) with the following sequences: Primer 1
861 – GTTCGTTGTGCCTCATTCG, Primer 2 – TCGGAACGTACTTCTGGAC, Probe –
862 AGGAATGCTTCAGCGCTG; and universal bacterial 16S rDNA was detected using Taqman
863 primer-probe sets with previously designed sequences (Nadkarni et al., 2002): Primer 1 –
864 GGACTACCAGGGTATCTAATCCTGTT, Primer 2 – TCCTACGGGAGGCAGCAGT, Probe –
865 CGTATTACCGCGGCTGCTGGCAC.

866 **RNAscope**

867 Swiss rolls of intestinal tissue were fixed in 10% neutral-buffered formalin for 18-24hr and
868 paraffin-embedded. Tissue sections (5μm) were cut and maintained at room temperature with
869 desiccant until staining. RNA *in situ* hybridization was performed using the RNAscope Multiplex
870 Fluorescent v2 kit (Advanced Cell Diagnostics, Newark, CA) per protocol guidelines. Staining with
871 anti-sense probes for detection of *Ifit1* (ACD, #500071-C2), *Usp18* (ACD, #524651-C1) and MRV
872 (ACD, #1030611-C1) was performed using ACDBio protocols and reagents. MRV probes were
873 designed to target 2-1683 of DQ391187 against NSP3, VP7, and NP4. Slides were stained with
874 DAPI and mounted with ProLong Gold antifade reagent (ThermoFisher), and imaged using a
875 Zeiss ApoTome2 on an Axio Imager, with a Zeiss AxioCam 506 (Zeiss).

876 Collected images were batch processed in Zeiss Zen 3.1 using unstained control slides to
877 set background values and quantified using ImageJ. Area of *Ifit1* was determined by positive *Ifit1*
878 fluorescent area relative to the total fluorescent area of the tissue section. *Ifit1*+ mRV-infected
879 cells were defined as mRV+ particles with greater than 5μm area with a maximum *Ifit1* intensity
880 greater than 10% above background. These *Ifit1*+ cells were then divided by the total number
881 mRV+ cells to determine the percentage of *Ifit1*+ mRV-infected cells.

882 **Flow Cytometry and Magnet Enrichment**

883 Dissociated cells were collected and stained for flow cytometry. Cells were stained with
884 Zombie Aqua viability dye (BioLegend), Fc receptor-blocking antibody (CD16/CD32; BioLegend),

885 anti-EpCAM (clone G8.8; BioLegend), and anti-CD45 (clone 30-F11; BioLegend). For analysis of
886 murine rotavirus infection, cells were stained with anti-rotavirus (polyclonal; ThermoFisher, #PA1-
887 7241) followed by goat anti-rabbit secondary (ThermoFisher). All data were analyzed using
888 FlowJo software (BD Biosciences). Gates were set based on unstained and single-fluorophore
889 stains. IECs were selected by gating on live, EpCAM-positive, CD45-negative cells. Gates for
890 murine rotavirus infection were set based on naïve samples.

891 Where indicated, dissociated cells were enriched using MojoSort Mouse anti-APC
892 Nanobeads (BioLegend, #480072) after flow cytometry staining for anti-EpCAM and anti-CD45
893 with APC fluorophores by following manufacturer protocols.

894 **RNA sequencing and expression analysis**

895 Wild-type C57BL/6J or *Ifnlr1*$^{-/-}$ mice were administered *ad libitum* Kool-aid or ABX for two
896 weeks, or wild-type mice were administered 25μg recombinant IFN-λ for one day, then ileal
897 segments lacking Peyer's patches were harvested and RNA sequencing was performed as prior
898 (Park et al., 2016). mRNA from ilea was purified with oligo-dT beads (Invitrogen, Carlsbad, CA)
899 and cDNA was synthesized using a custom oligo-dT primer containing a barcode and adaptor-
900 linker sequence, degradation of RNA-DNA hybrid following single-strand synthesis, and ligation
901 of a second sequencing linker with T4 ligase (New England Biolabs, Ipswich, MA). These
902 reactions were cleaned up by solid phase reversible immobilization (SPRI), followed by
903 enrichment by PCR and further SPRI to yield strand-specific RNA-seq libraries. Libraries were
904 sequenced with an Illumina HiSeq 2500 with three to four mice were included in each group.
905 Samples were demultiplexed with second mate, reads were aligned with STAR aligner and then
906 counted with HT-Seq. Differentially expressed genes were identified using DESeq2 (Love et al.,
907 2014) based on cutoffs of 2-fold change, and an inclusive p-value < 0.5. Standard gene set
908 enrichment analysis was performed to identify enrichments in IFN-λ response genes. RNA-seq
909 data were uploaded to the European Nucleotide Archive (accession #: PRJEB43446).

910 **16S rRNA gene Illumina sequencing and analysis**

911 For sequencing of the 16S rRNA gene, primer selection and PCRs were performed as
912 described previously (Caporaso et al., 2011). Briefly, each sample was amplified in triplicate with
913 Golay-barcoded primers specific for the V4 region (F515/R806), combined, and confirmed by gel
914 electrophoresis. PCR reactions contained 18.8μL RNase/DNase-free water, 2.5μL of 10X High
915 Fidelity PCR Buffer (Invitrogen, 11304-102), 0.5μL of 10 mM dNTPs, 1μL 50 of mM MgSO4, 0.5μL
916 each of forward and reverse primers (10 μM final concentration), 0.1μL of Platinum High Fidelity
917 Taq (Invitrogen, 11304-102), and 1.0μL genomic DNA. Reactions were held at 94°C for 2 min to
918 denature the DNA, with amplification proceeding for 26 cycles at 94°C for 15 s, 50°C for 30 s, and
919 68°C for 30 s; a final extension of 2 min at 68°C was added to ensure complete amplification.
920 Amplicons were pooled and purified with 0.6x Agencourt AMPure XP beads (Beckman-Coulter,
921 A63882) according to the manufacturer's instructions. The final pooled samples, along with
922 aliquots of the three sequencing primers, were sent to the DNA Sequencing Innovation Lab
923 (Washington University School of Medicine) for sequencing by the 2 X 250bp protocol with the
924 Illumina MiSeq platform.

925 Read quality control and the resolution of amplicon sequence variants were performed in
926 R with DADA2 (Callahan et al., 2016). Non-bacterial amplicon sequence variants were filtered
927 out. The remaining reads were assigned taxonomy using the Ribosomal Database Project (RDP
928 trainset 16/release 11.5) 16S rRNA gene sequence database (Cole et al., 2014). Ecological
929 analyses, such as alpha-diversity (richness, Shannon diversity) and beta-diversity analyses
930 (UniFrac distances), were performed using PhyloSeq and additional R packages (McMurdie and
931 Holmes, 2013). 16S sequencing data have been uploaded to the European Nucleotide Archive
932 (accession #: PRJEB43446).

933 **Single-cell RNA Sequencing Analyses**

934 A mouse single-cell RNA sequencing dataset generated by Haber et al. was accessed
935 from NCBI's Gene Expression Omnibus (GEO), accession #: GSE92332. A human pediatric
936 single-cell RNA sequencing dataset generated by Elmentaite et al. was accessed in processed

form from The Gut Cell Atlas, with raw data also available on EMBL-EBI Array Express, accession #: E-MTAB-8901. Files were analyzed in R using Seurat (v. 3.2.2) (Stuart and Butler et al., 2019). For the Haber et al. dataset, UMI counts were normalized to counts per million, log2 transformed, and homeostatic ISGs were selected for analysis. Data was collated by previously annotated cell-type and proportion of cells expressing each individual ISG was calculated. For Elmentaite et al, data was restricted to healthy controls and then collated by previously annotated cell-type to determine the proportion of cells expressing individual ISGs.

Statistical Analyses

Sample size estimation was performed based on historical data. Data were analyzed with Prism software (GraphPad Prism Software), with specified tests as noted in the figure legends.

Data availability.

RNA sequencing data obtained in this study have been deposited in the European Nucleotide Archive (accession #: PRJEB43446).

Acknowledgments

The authors would like to thank the following OHSU core facilities: Integrated Genomics Laboratory, Advanced Light Microscopy Core, and Histopathology Core; and the following WUSTL core facilities: Genome Technology Access Center. T.J.N. was supported NIH grant R01-AI130055 and by a faculty development award from the Sunlin & Priscilla Chou Foundation. J.A.V. was supported by NIH grants T32-GM071338 and T32-AI007472. M.T.B. was supported by NIH grants R01-AI139314, R01-AI141716, and R01-AI141478, the Pew Biomedical Scholars Program of the Pew Charitable Trusts, and a Children's Discovery Institute of Washington University and St. Louis Children's Hospital Interdisciplinary Research Initiative grant (MI-II-2019–790). The funders had no role in study design, data collection and interpretation, or the decision to submit the work for publication.

Author Contributions

Conceptualization, J.A.V., M.T.B., and T.J.N.; Methodology, J.A.V., M.T.B., and T.J.N.; Investigation, J.A.V., S.T.P., E.A.K., M.W., H.I., R.R., C.D., D.C., A.W., M.A., S.L., and T.J.N.; Writing – Original Draft, J.A.V.; Writing – Review & Editing, J.A.V., M.T.B., and T.J.N.; Visualization, J.A.V.; Supervision, M.T.B. and T.J.N.; Project Administration, L.L., M.T.B., and T.J.N.; Funding Acquisition, M.T.B. and T.J.N.

Disclosure

We declare no competing interests.

References

Abt, M.C., Osborne, L.C., Monticelli, L.A., Doering, T.A., Alenghat, T., Sonnenberg, G.F., Paley, M.A., Antenus, M., Williams, K.L., Erikson, J., et al. (2012). Commensal bacteria calibrate the activation threshold of innate antiviral immunity. Immunity *37*, 158–170.

Arnold, M.M., Sen, A., Greenberg, H.B., and Patton, J.T. (2013). The battle between rotavirus and its host for control of the interferon signaling pathway. PLoS Pathog. *9*, e1003064.

Atuma, C., Strugala, V., Allen, A., and Holm, L. (2001). The adherent gastrointestinal mucus gel layer: thickness and physical state in vivo. Am. J. Physiol. Gastrointest. Liver Physiol. *280*, G922-9.

Baldridge, M.T., Nice, T.J., McCune, B.T., Yokoyama, C.C., Kambal, A., Wheadon, M., Diamond, M.S., Ivanova, Y., Artyomov, M., and Virgin, H.W. (2015). Commensal microbes and interferon-λ determine persistence of enteric murine norovirus infection. Science *347*, 266–269.

Baldridge, M.T., Lee, S., Brown, J.J., McAllister, N., Urbanek, K., Dermody, T.S., Nice, T.J., and Virgin, H.W. (2017). Expression of Ifnlr1 on Intestinal Epithelial Cells Is Critical to the Antiviral Effects of Interferon Lambda against Norovirus and Reovirus. J. Virol. *91*, JVI.02079-16.

Bradley, K.C., Finsterbusch, K., Schnepf, D., Crotta, S., Llorian, M., Davidson, S., Fuchs, S.Y., Staeheli, P., and Wack, A. (2019). Microbiota-Driven Tonic Interferon Signals in Lung Stromal Cells Protect from Influenza Virus Infection. Cell Rep. *28*, 245-256.e4.

Burns, J.W., Krishnaney, A.A., Vo, P.T., Rouse, R. V., Anderson, L.J., and Greenberg, H.B. (1995). Analyses of homologous rotavirus infection in the mouse model. Virology *207*, 143–153.

Callahan, B.J., McMurdie, P.J., Rosen, M.J., Han, A.W., Johnson, A.J.A., and Holmes, S.P. (2016). DADA2: High-resolution sample inference from Illumina amplicon data. Nat. Methods *13*, 581–583.

Caporaso, J.G., Lauber, C.L., Walters, W.A., Berg-Lyons, D., Lozupone, C.A., Turnbaugh, P.J., Fierer, N., and Knight, R. (2011). Global patterns of 16S rRNA diversity at a depth of millions of sequences per sample. Proc. Natl. Acad. Sci. *108*, 4516–4522.

Chieppa, M., Rescigno, M., Huang, A.Y.C., and Germain, R.N. (2006). Dynamic imaging of dendritic cell extension into the small bowel lumen in response to epithelial cell TLR engagement. J. Exp. Med. *203*, 2841–2852.

Chu, H., and Mazmanian, S.K. (2013). Innate immune recognition of the microbiota promotes host-microbial symbiosis. Nat. Immunol. *14*, 668–675.

Cole, J.R., Wang, Q., Fish, J.A., Chai, B., McGarrell, D.M., Sun, Y., Brown, C.T., Porras-Alfaro, A., Kuske, C.R., and Tiedje, J.M. (2014). Ribosomal Database Project: data and tools for high throughput rRNA analysis. Nucleic Acids Res. *42*, D633-42.

Elmentaite, R., Ross, A.D.B., Roberts, K., James, K.R., Ortmann, D., Gomes, T., Nayak, K., Tuck, L., Pritchard, S., Bayraktar, O.A., et al. (2020). Single-Cell Sequencing of Developing Human Gut Reveals Transcriptional Links to Childhood Crohn's Disease. Dev. Cell *55*, 771-783.e5.

Fenaux, M., Cuadras, M.A., Feng, N., Jaimes, M., and Greenberg, H.B. (2006). Extraintestinal spread and replication of a homologous EC rotavirus strain and a heterologous rhesus rotavirus in BALB/c mice. J. Virol. *80*, 5219–5232.

Ganal, S.C., Sanos, S.L., Kallfass, C., Oberle, K., Johner, C., Kirschning, C., Lienenklaus, S., Weiss, S., Staeheli, P., Aichele, P., et al. (2012). Priming of natural killer cells by nonmucosal mononuclear phagocytes requires instructive signals from commensal microbiota. Immunity *37*,

1016 171–186.

1017 Haber, A.L., Biton, M., Rogel, N., Herbst, R.H., Shekhar, K., Smillie, C., Burgin, G., Delorey,
1018 T.M., Howitt, M.R., Katz, Y., et al. (2017). A single-cell survey of the small intestinal epithelium.
1019 Nature *551*, 333–339.

1020 Hakim, M.S., Chen, S., Ding, S., Yin, Y., Ikram, A., Ma, X.X., Wang, W., Peppelenbosch, M.P.,
1021 and Pan, Q. (2018). Basal interferon signaling and therapeutic use of interferons in controlling
1022 rotavirus infection in human intestinal cells and organoids. Sci. Rep. *8*, 1–13.

1023 Hernández, P.P., Mahlakoiv, T., Yang, I., Schwierzeck, V., Guendel, F., Gronke, K., Ryffel, B.,
1024 Dumoutier, L., Renauld, J., and Suerbaum, S. (2015). Interferon-λ and interleukin-22 cooperate
1025 for the induction of interferon-stimulated genes and control of rotavirus infection. Nat. Immunol.
1026 *16*, 698–707.

1027 Honda, K., and Littman, D.R. (2016). The microbiota in adaptive immune homeostasis and
1028 disease. Nature *535*, 75–84.

1029 Honda, K., Yanai, H., Negishi, H., Asagiri, M., Sato, M., Mizutani, T., Shimada, N., Ohba, Y.,
1030 Takaoka, A., Yoshida, N., et al. (2005a). IRF-7 is the master regulator of type-I interferon-
1031 dependent immune responses. Nature *434*, 772–777.

1032 Honda, K., Ohba, Y., Yanai, H., Negishi, H., Mizutani, T., Takaoka, A., Taya, C., and Taniguchi,
1033 T. (2005b). Spatiotemporal regulation of MyD88-IRF-7 signalling for robust type-I interferon
1034 induction. Nature *434*, 1035–1040.

1035 Ingle, H., Peterson, S.T., and Baldridge, M.T. (2018). Distinct Effects of Type I and III
1036 Interferons on Enteric Viruses. Viruses *10*.

1037 Ingle, H., Hassan, E., Gawron, J., Mihi, B., Li, Y., Kennedy, E.A., Kalugotla, G., Makimaa, H.,
1038 Lee, S., Desai, P., et al. (2021). Murine astrovirus tropism for goblet cells and enterocytes
1039 facilitates an IFN-λ response in vivo and in enteroid cultures. Mucosal Immunol. *14*, 751–761.

1040 Iwasaki, A., and Medzhitov, R. (2015). Control of adaptive immunity by the innate immune
1041 system. Nat. Immunol. *16*, 343–353.

1042 Johansson, M.E. V., Larsson, J.M.H., and Hansson, G.C. (2011). The two mucus layers of colon
1043 are organized by the MUC2 mucin, whereas the outer layer is a legislator of host-microbial
1044 interactions. Proc. Natl. Acad. Sci. *108*, 4659–4665.

1045 Kim, S., Covington, A., and Pamer, E.G. (2017). The intestinal microbiota: Antibiotics,
1046 colonization resistance, and enteric pathogens. Immunol. Rev. *279*, 90–105.

1047 Kotenko, S. V, and Durbin, J.E. (2017). Contribution of type III interferons to antiviral immunity:
1048 Location, Location, Location. J. Biol. Chem. *292*, 7295–7303.

1049 Krajmalnik-Brown, R., Ilhan, Z.E., Kang, D.W., and DiBaise, J.K. (2012). Effects of gut microbes
1050 on nutrient absorption and energy regulation. Nutr. Clin. Pract. *27*, 201–214.

1051 Levy, D.E., and García-Sastre, A. (2001). The virus battles: IFN induction of the antiviral state
1052 and mechanisms of viral evasion. Cytokine Growth Factor Rev. *12*, 143–156.

1053 Liberzon, A., Birger, C., Thorvaldsdóttir, H., Ghandi, M., Mesirov, J.P., and Tamayo, P. (2016).
1054 The Molecular Signatures Database (MSigDB) hallmark gene set collection. Cell Syst. *1*, 417–
1055 425.

1056 Lin, J.-D., Feng, N., Sen, A., Balan, M., Tseng, H.-C., McElrath, C., Smirnov, S. V., Peng, J.,
1057 Yasukawa, L.L., Durbin, R.K., et al. (2016). Distinct Roles of Type I and Type III Interferons in
1058 Intestinal Immunity to Homologous and Heterologous Rotavirus Infections. PLoS Pathog. *12*,
1059 e1005600.

1060 Love, M.I., Huber, W., and Anders, S. (2014). Moderated estimation of fold change and
1061 dispersion for RNA-seq data with DESeq2. Genome Biol. *15*, 550.

1062 Mahlakõiv, T., Hernandez, P., Gronke, K., Diefenbach, A., and Staeheli, P. (2015). Leukocyte-
1063 derived IFN-α/β and epithelial IFN-λ constitute a compartmentalized mucosal defense system
1064 that restricts enteric virus infections. PLoS Pathog. *11*, e1004782.

1065 McDole, J.R., Wheeler, L.W., McDonald, K.G., Wang, B., Konjufca, V., Knoop, K.A., Newberry,
1066 R.D., and Miller, M.J. (2012). Goblet cells deliver luminal antigen to CD103 + dendritic cells in
1067 the small intestine. Nature *483*, 345–349.

1068 McMurdie, P.J., and Holmes, S. (2013). phyloseq: an R package for reproducible interactive
1069 analysis and graphics of microbiome census data. PLoS One *8*, e61217.

1070 Monroe, K.M., McWhirter, S.M., and Vance, R.E. (2010). Induction of type I interferons by
1071 bacteria. Cell. Microbiol. *12*, 881–890.

1072 Nadkarni, M., Martin, F.E., Jacques, N.A., and Hunter, N. (2002). Determination of bacterial load
1073 by real-time PCR using a broad range (universal) probe and primer set. Microbiology *148*, 257–
1074 266.

1075 Nice, T.J., Baldridge, M.T., McCune, B.T., Norman, J.M., Lazear, H.M., Artyomov, M., Diamond,
1076 M.S., and Virgin, H.W. (2015). Interferon-λ cures persistent murine norovirus infection in the
1077 absence of adaptive immunity. Science *347*, 269–273.

1078 Nice, T.J., Osborne, L.C., Tomov, V.T., Artis, D., Wherry, E.J.J., and Virgin, H.W. (2016). Type I
1079 Interferon Receptor Deficiency in Dendritic Cells Facilitates Systemic Murine Norovirus
1080 Persistence Despite Enhanced Adaptive Immunity. PLoS Pathog. *12*, e1005684.

1081 Niess, J.H., Brand, S., Gu, X., Landsman, L., Jung, S., McCormick, B.A., Vyas, J.M., Boes, M.,
1082 Ploegh, H.L., Fox, J.G., et al. (2005). CX3CR1-mediated dendritic cell access to the intestinal
1083 lumen and bacterial clearance. Science *307*, 254–258.

1084 Odendall, C., Voak, A.A., and Kagan, J.C. (2017). Type III IFNs Are Commonly Induced by
1085 Bacteria-Sensing TLRs and Reinforce Epithelial Barriers during Infection. J. Immunol. *199*,
1086 3270–3279.

1087 Osterlund, P.I., Pietilä, T.E., Veckman, V., Kotenko, S. V, and Julkunen, I. (2007). IFN
1088 regulatory factor family members differentially regulate the expression of type III IFN (IFN-
1089 lambda) genes. J. Immunol. *179*, 3434–3442.

1090 Park, S., Buck, M.D., Desai, C., Zhang, X., Loginicheva, E., Martinez, J., Freeman, M.L., Saitoh,
1091 T., Akira, S., Guan, J.L., et al. (2016). Autophagy Genes Enhance Murine Gammaherpesvirus
1092 68 Reactivation from Latency by Preventing Virus-Induced Systemic Inflammation. Cell Host
1093 Microbe *19*, 91–101.

1094 Pott, J., Mahlakoiv, T., Mordstein, M., Duerr, C.U., Michiels, T., Stockinger, S., Staeheli, P., and
1095 Hornef, M.W. (2011). IFN-λ determines the intestinal epithelial antiviral host defense. Proc. Natl.
1096 Acad. Sci. *108*, 7944–7949.

1097 Rojas, J.M., Alejo, A., Martín, V., and Sevilla, N. (2021). Viral pathogen-induced mechanisms to
1098 antagonize mammalian interferon (IFN) signaling pathway. Cell. Mol. Life Sci. *78*, 1423–1444.

1099 Rooks, M.G., and Garrett, W.S. (2016). Gut microbiota, metabolites and host immunity. Nat.
1100 Rev. Immunol. *16*, 341–352.

1101 Sadler, A.J., and Williams, B.R.G. (2008). Interferon-inducible antiviral effectors. Nat. Rev.
1102 Immunol. *8*, 559–568.

1103 Schmid, S., Mordstein, M., Kochs, G., García-Sastre, A., and TenOever, B.R. (2010).

1104 Transcription factor redundancy ensures induction of the antiviral state. J. Biol. Chem. *285*,
1105 42013–42022.

1106 Schneider, W.M., Chevillotte, M.D., and Rice, C.M. (2014). Interferon-stimulated genes: a
1107 complex web of host defenses. Annu. Rev. Immunol. *32*, 513–545.

1108 Schoggins, J.W., and Rice, C.M. (2011). Interferon-stimulated genes and their antiviral effector
1109 functions. Curr. Opin. Virol. *1*, 519–525.

1110 Shi, Z., Zou, J., Zhang, Z., Zhao, X., Noriega, J., Zhang, B., Zhao, C., Ingle, H., Bittinger, K.,
1111 Mattei, L.M., et al. (2019). Segmented Filamentous Bacteria Prevent and Cure Rotavirus
1112 Infection. Cell *179*, 644-658.e13.

1113 Sommereyns, C., Paul, S., Staeheli, P., and Michiels, T. (2008). IFN-Lambda (IFN-λ) Is
1114 Expressed in a Tissue-Dependent Fashion and Primarily Acts on Epithelial Cells In Vivo. PLoS
1115 Pathog. *4*, e1000017.

1116 Steed, A.L., Christophi, G.P., Kaiko, G.E., Sun, L., Goodwin, V.M., Jain, U., Esaulova, E.,
1117 Artyomov, M.N., Morales, D.J., Holtzman, M.J., et al. (2017). The microbial metabolite
1118 desaminotyrosine protects from influenza through type I interferon. Science (80-.). *357*, 498–
1119 502.

1120 Stefan, K.L., Kim, M. V, Iwasaki, A., and Kasper, D.L. (2020). Commensal Microbiota
1121 Modulation of Natural Resistance to Virus Infection. Cell *183*, 1312-1324.e10.

1122 Stockinger, S., Duerr, C.U., Fulde, M., Dolowschiak, T., Pott, J., Yang, I., Eibach, D., Bäckhed,
1123 F., Akira, S., Suerbaum, S., et al. (2014). TRIF signaling drives homeostatic intestinal epithelial
1124 antimicrobial peptide expression. J. Immunol. *193*, 4223–4234.

1125 Stuart, T., Butler, A., Hoffman, P., Hafemeister, C., Papalexi, E., Mauck, W.M., Hao, Y.,
1126 Stoeckius, M., Smibert, P., and Satija, R. (2019). Comprehensive Integration of Single-Cell
1127 Data. Cell *177*, 1888-1902.e21.

1128 Swamy, M., Abeler-Dörner, L., Chettle, J., Mahlakõiv, T., Goubau, D., Chakravarty, P., Ramsay,
1129 G., Reis e Sousa, C., Staeheli, P., Blacklaws, B.A., et al. (2015). Intestinal intraepithelial
1130 lymphocyte activation promotes innate antiviral resistance. Nat. Commun. *6*, 7090.

1131 Taylor, K.E., and Mossman, K.L. (2013). Recent advances in understanding viral evasion of
1132 type I interferon. Immunology *138*, 190–197.

1133 Thompson, M.R., Kaminski, J.J., Kurt-Jones, E.A., and Fitzgerald, K.A. (2011). Pattern
1134 recognition receptors and the innate immune response to viral infection. Viruses *3*, 920–940.

1135 Tomasello, E., Naciri, K., Chelbi, R., Bessou, G., Fries, A., Gressier, E., Abbas, A., Pollet, E.,
1136 Pierre, P., Lawrence, T., et al. (2018). Molecular dissection of plasmacytoid dendritic cell
1137 activation in vivo during a viral infection. EMBO J. *37*, 1–19.

1138 Uchiyama, R., Chassaing, B., Zhang, B., and Gewirtz, A.T. (2014). Antibiotic treatment
1139 suppresses rotavirus infection and enhances specific humoral immunity. J. Infect. Dis. *210*,
1140 171–182.

1141 Williams, J.M., Duckworth, C.A., Burkitt, M.D., Watson, A.J.M., Campbell, B.J., and Pritchard,
1142 D.M. (2015). Epithelial cell shedding and barrier function: a matter of life and death at the small
1143 intestinal villus tip. Vet. Pathol. *52*, 445–455.

1144 Van Winkle, J.A., Constant, D.A., Li, L., and Nice, T.J. (2020). Selective Interferon Responses
1145 of Intestinal Epithelial Cells Minimize Tumor Necrosis Factor Alpha Cytotoxicity. J. Virol. *94*,
1146 e00603-20.

1147 Winkler, E.S., Shrihari, S., Hykes, B.L., Handley, S.A., Andhey, P.S., Huang, Y.-J.S., Swain, A.,

1148 Droit, L., Chebrolu, K.K., Mack, M., et al. (2020). The Intestinal Microbiome Restricts Alphavirus
1149 Infection and Dissemination through a Bile Acid-Type I IFN Signaling Axis. Cell *182*, 901-
1150 918.e18.

1151 Zhang, B., Chassaing, B., Shi, Z., Uchiyama, R., Zhang, Z., Denning, T.L., Crawford, S.E.,
1152 Pruijssers, A.J., Iskarpatyoti, J.A., Estes, M.K., et al. (2014). Viral infection. Prevention and cure
1153 of rotavirus infection via TLR5/NLRC4-mediated production of IL-22 and IL-18. Science (80-.).
1154 *346*, 861–865.

1155